國立交通大學

多媒體工程研究所

碩 士 論 文

模擬退火於圖形偵測及震測圖形上之應用

Simulated Annealing for Pattern Detection and Seismic Applications

研 究 生：陳楷儒

指導教授：黃國源 教授

中 華 民 國 九 十 六 年 六 月

模擬退火於圖形偵測及震測圖形上之應用

學生：陳楷儒　　指導教授：黃國源教授

國立交通大學多媒體工程研究所碩士班

摘要

關鍵詞：模擬退火、全域最佳化、類神經網路、Hough 轉換、震測圖形。

我們提出一個運用模擬退火演算法的參數偵測系統來偵測影像中的直線、圓、橢圓與雙曲線，並且將此系統應用到震測圖形的偵測上。在此系統中，我們定義了點到雙曲線的距離使得系統能夠成功的運作。這個模擬退火的參數偵測系統能找到一組圖形(直線、圓、橢圓、與雙曲線)的參數，使得影像上的點到這組圖形的距離爲最小。除此之外，我們利用平均的最小距離作爲判斷的依據，提出自動判斷影像中圖形數量的方法。在實驗的部分，對於影像中的直線、圓、橢圓與雙曲線均能成功的偵測。此系統也應用於偵測模擬與真實的單炸點震測圖形中直接波的直線與反射波的雙曲線，此結果將幫助震測圖形的解釋與進一步的震測圖形處理。

Simulated Annealing or Pattern Detection and Seismic Applications

Student: Kai-Ju Chen Advisor: Dr. Kou-Yuan Huang

Institute of Multimedia Engineering
National Chiao Tung University

ABSTRACT

Keywords: simulated annealing, global optimization, neural network, Hough transform, seismic pattern.

Simulated annealing algorithm is adopted to detect the parameters of ellipses, hyperbolas and lines in images and applied to seismic pattern detection. We define the distance from a point to a hyperbolic pattern such that the detection becomes feasible. The proposed simulated annealing parameter detection system has the capability of searching a set of parameter vectors with global minimal error with respect to the input data. Based on the average of the minimum distance, we propose a method to determine the number of patterns automatically. Experiments on the detection of ellipses, hyperbolas, circles and lines in images are quite successful. The detection system is also applied to detect the line pattern of direct wave and the hyperbolic pattern of reflection wave in the simulated and real one-shot seismogram. The results can improve seismic interpretations and further seismic data processing.

誌　　謝

感謝我的指導老師，黃國源教授。老師的辛勤指導與勉勵，使我得以順利完成此論文。同時感謝參與口試的口試委員，劉長遠教授、蘇豐文教授以及王榮華教授，由於您們的指導與建議，讓這篇論文更加完整和充實。

感謝Colorado School of Mine發展的Seismic Unix軟體與國科會的支持，讓本計畫NSC 95-2221-E-009-221得以順利完成。

感謝我的家人，謝謝你們在全心全意地支持，讓我在這研究的路上走得更順利，進而能無後顧之憂的學習，追求理想。感謝我的同學與朋友，在生活與學業上互相勉勵，共同成長。

謹向所有支持我、勉勵我的師長與親友，致上最誠摯的祝福，謝謝你們!

Contents

List of Figures

List of Tables

Chapter 1

Introduction

Traditionally, the Hough transform (HT) is used to detect the parametric patterns such as lines and circles by mapping points in the image into the parameter space and find the peak (maximum) in the parameter space [1]-[2]. The coordinate of the peak in parameter space corresponds to a pattern in the image space.

Seismic pattern recognition plays an important role in oil exploration. In seismic data, a line represents the direct wave and a hyperbola represents the reflection wave [3]-[5]. In 1985, Huang et al. had applied the HT to detect line pattern of direct wave and hyperbolic pattern of reflection wave in a one-shot seismogram [7]. However, it was not easy to determine the peak in the parameter space and the large memory requirement was also a problem.

The Hough transform neural network (HTNN) was developed to solve the traditional HT problem [8]. It was designed to detect lines, circles, and ellipses by gradient descent to minimize the distance between points and patterns. HTNN was also adopted to detect lines and hyperbolas in a one-shot seismogram by Huang et al. [9]. The iterative method required less memory, but it had local minimum problem.

Simulated annealing (SA) was first proposed by Kirkpatrick in 1983 [10]. The algorithm simulates the procedure of the substance frozen from melt to a perfect crystal or low-energy state by careful annealing. The Metropolis criterion [11] which conditionally allows the state of the system to higher energy condition is the key of the SA algorithm to reach the global minimum. SA algorithm solves many combinatorial problems such as traveling salesman problem, circuit wiring problem, and clustering problem [10], [12]-[16]. In 1987, Corana et al. applied the SA algorithm to solve the global optimal solution of the continuous function [17] and compare it with simplex method [18] and adaptive random search [19]. The result shows the power of SA algorithm.

Here, we take the advantage of global optimization in SA to minimize the distance between points and patterns to detect parametric patterns: circles, ellipses, hyperbolas and lines. Also the proposed detection system is applied to the detection of line

pattern of direct wave and hyperbolic pattern of reflection wave in the simulated and real one-shot seismogram.

Chapter 2

Simulated Annealing

Optimization by SA is first proposed by Kirkpatrick et al. in 1983 to solve combinatorial problem such as the placement and circuit wiring in chip design and traveling salesmen problem [10]. The algorithm compares the optimization problem to cooling a fluid. A regular crystal has all atoms in the ground state or the lowest energy state by careful cooling procedure. In the procedure, the state of atoms is conditionally allowed to a higher energy state. Similarly, to achieve the optimal solution, the algorithm has to accept a solution with larger error in the procedure based on a criterion, Metropolis criterion [11]. Fig. 1 illustrates the function $F(x)$ and the descent and ascent direction at x_1. For the gradient descent algorithm, the direction for the next step is always descent. On the other hand, SA algorithm conditionally chooses ascent direction and this allows it to reach global minimum. The main steps of SA algorithm are in the following.

Algorithm: SA algorithm to get a configuration with lowest energy state.
Input: A system with unknown minimum-energy configuration.
Output: A minimum-energy configuration.

Step 1: Initialization:

1. Set the initial temperature.
2. Set the initial configuration.
3. Define the temperature decreasing function.
4. Define the energy function.

Step 2: Give the configuration a random displacement then obtain a new configuration and a resulting energy change ΔE. To accept the displaced configuration or not is determined by Metropolis criterion. Metropolis criterion is a rule: If $\Delta E \leq 0$, the displaced configuration is accepted and treated as the starting configuration of the next step.

On the other hand, if $\Delta E \geq 0$, the acceptance of the displaced configuration is treated probabilistically:

1. Calculate $prob = \exp[-\Delta E/T(t)]$.
2. Generate a random number x. For convenience, random numbers uniformly distributed over (0, 1) are chosen.

3. If *prob* is greater than *x*, the new configuration is retained. Otherwise, the original configuration is used to the starting configuration of the next step.

Repeat this step until equilibrium condition.

Step 3: When the equilibrium condition is reached, cool the system using the temperature decreasing function. Repeat this step until frozen condition.

In the SA algorithm, when to reach equilibrium condition and frozen condition is determined prior. For example, in step 2, the system reaches equilibrium condition in a specific temperature after 100 trials. Similarly, in step 3, frozen condition can be the temperature $T < 0.001$. Fig. 2 is the flowchart of the SA algorithm.

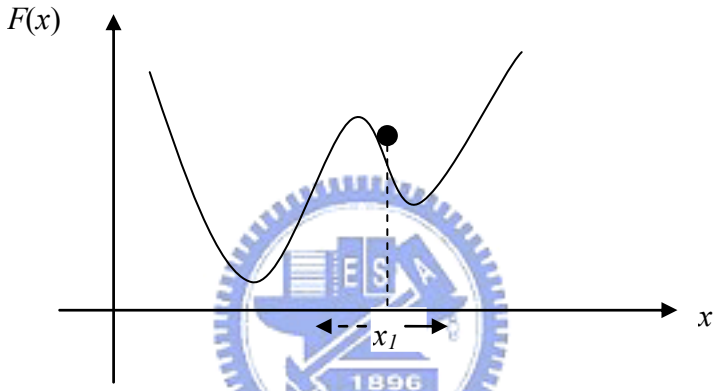

Fig. 1. Illustration of descent and ascent direction. Dash arrow: ascent direction. Solid arrow: descent direction.

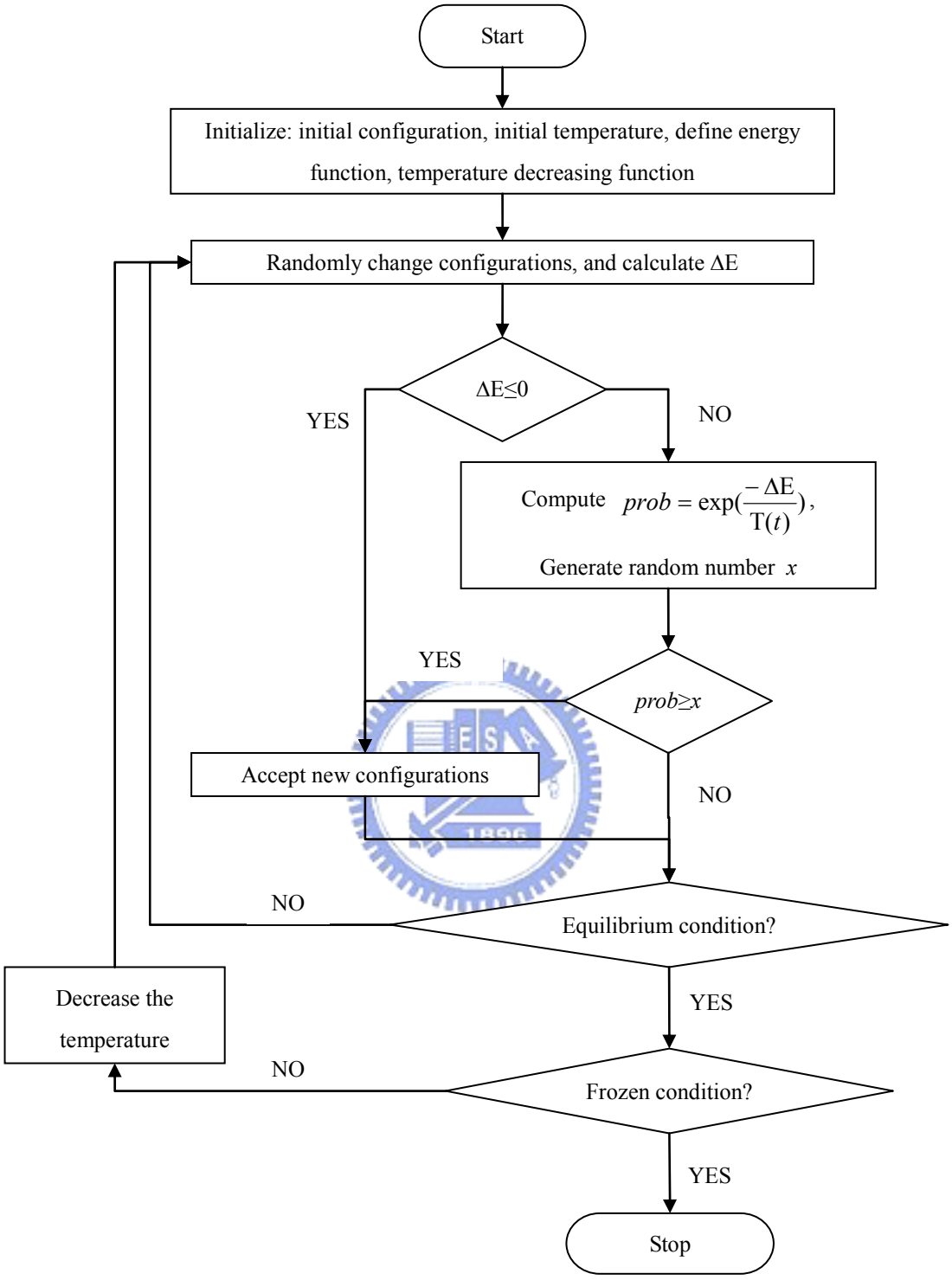

Fig. 2. Flowchart of the simulated annealing algorithm.

Chapter 3

Proposed System

Fig. 3 is the overview of the proposed system. The detection system takes the N data as the input, followed by the SA parameter detection system to detect a set of parameter vectors of K patterns. After convergence, patterns are recovered from the detected parameter vectors.

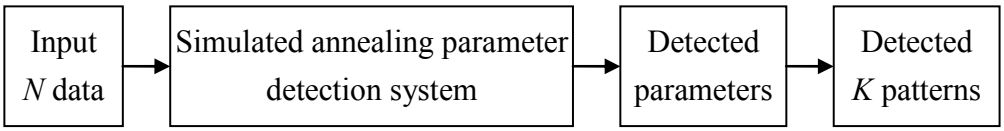

Fig. 3. The system overview.

SA parameter detection system consists of two main parts: 1. definition of system error (energy, distance); 2. SA algorithm for determination of the parameter vectors with minimum error. To obtain the system error, we calculate the error or the distance from a point to patterns, and combine the errors from all points to patterns to be the system error.

3.1 *Definition of the system error*

To define the error or energy of the system, we first discuss the equation of the quadratic curve and the distance from a point to the pattern. Seconds, the error from a point to K patterns is the geometric mean of the distances from the point to all individual patterns. Finally, the system error is the arithmetic mean of the error of N points.

3.1.1 Equation of the parametric pattern

Circles, ellipses, and hyperbolas with rotations and translations can be expressed in the standard form in the translated and rotated coordinate system. That is, in translated and rotated coordinate system x''-y'', circles, ellipses, and hyperbolas can be expressed in the standard form as

$$ax''^2 + by''^2 = f\ , \tag{1}$$

where a, b, and f control the graph of the equation. Table I lists the relation between the graph of the equation and parameters a, b, and f. If $a > 0$, $b > 0$, and $f > 0$ or $a < 0$, $b < 0$, and $f < 0$, the graph is an ellipse; if $a > 0$, $b < 0$, and $f \neq 0$ or $a < 0$, $b > 0$, and $f \neq 0$ the graph is a hyperbola. If $a > 0$, $b < 0$, and $f = 0$ or $a < 0$, $b > 0$, and $f = 0$, the graph represents the asymptotes of the hyperbola.

Table I

Relation between graph and parameters in (1)

a	b	f	Graph
+	+	+	Ellipse
−	−	+	No graph
+	−	+	Hyperbola
−	+	+	Hyperbola
+	−	−	Hyperbola
−	+	−	Hyperbola
+	+	−	No graph
−	−	−	Ellipse
+	−	0	Asymptote
−	+	0	Asymptote
+	+	0	Point
−	−	0	Point

Since x''-y'' are the axes counter-clockwise rotated by θ from x'- y', the relations of axes rotation are

$$\begin{aligned} x'' &= x'\cos\theta + y'\sin\theta \\ y'' &= -x'\sin\theta + y'\cos\theta . \end{aligned} \tag{2}$$

Fig. 4 illustrates the relation. The equation of ellipses and hyperbolas after axes being rotated back to x'- y' becomes

$$a[x'\cos\theta + y'\sin\theta]^2 + b[-x'\sin\theta + y'\cos\theta]^2 = f . \tag{3}$$

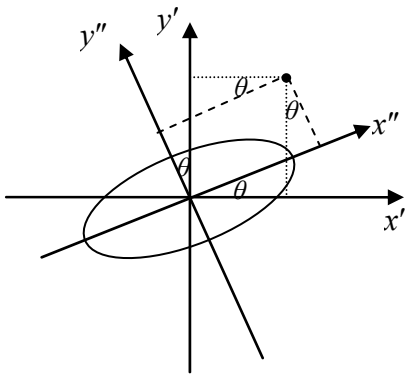

Fig. 4. Illustration of axis rotation: rotate the axis counterclockwise by θ.

Since x' and y' axes translates the origin of x-y coordinate system to (m_x, m_y), the relations of translation are

$$\begin{aligned} x' &= x - m_x \\ y' &= y - m_y \end{aligned}. \tag{4}$$

Fig. 5 illustrates the axes translation. And the equation in the x-y coordinate system is

$$a[(x-m_x)\cos\theta + (y-m_y)\sin\theta]^2 + b[-(x-m_x)\sin\theta + (y-m_y)\cos\theta]^2 = f\ . \tag{5}$$

This can completely express any translated and rotated ellipse or hyperbola in 2D space.

So we can use (5) to represents any ellipse and hyperbola with the parameter, a, b, f, θ, m_x, and m_y. Parameter (m_x, m_y) is the center; a, b, and θ are concerned about the shape; f is related to the size. In the matrix form, a parameter vector, $\mathbf{p} = [m_x, m_y, a, b, \theta, f]^T$ represents a pattern. Since (5) represents the asymptotes or two crossing lines when $f = 0$, we can use it to detect lines.

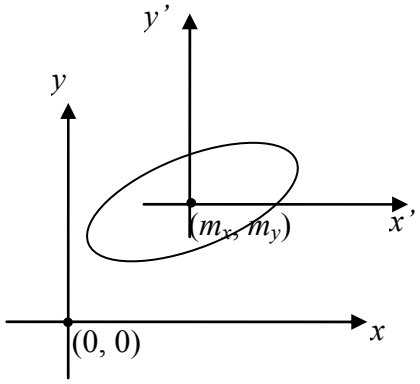

Fig. 5. Illustration of translation: translate the origin to (m_x, m_y).

3.1.2 Distance from a point to a pattern

Here, the detected patterns include ellipses, circles, hyperbolas, and lines. The distance from a point $\mathbf{x}_i$ to the kth pattern is defined as

$$d_k(x_i, y_i) = | a_k[(x_i - m_{k,x})\cos\theta_k + (y_i - m_{k,y})\sin\theta_k]^2 + b_k[-(x_i - m_{k,x})\sin\theta_k + (y_i - m_{k,y})\cos\theta_k]^2 - f_k | \quad (6)$$

Distance measure in (6) has a minimum $d(x_i, y_i) = 0$ when $a = 0$, $b = 0$, and $f = 0$. However, these are not our desired parameters. Also, the distance from a point to the pattern is affected by the scale of coefficients. So we have to normalize the parameter a and b.

Fig. 6 (a) illustrates the distance from points to the circle, $x^2 + y^2 = 1$. Fig. 7 (a) shows the distance from points to the ellipse, $0.5x^2 + 2y^2 = 1$. Fig. 8 (a) illustrates the distance from points to the hyperbola $x^2 - y^2 = 1$. Equal distance curves in those figures have corresponding distance 0.5, 1, 2, 5, 10, and 20. Fig. 6 (b) shows the distance from points to the circle $0.25x^2 + 0.25y^2 = 0.25$, which has the same shape with that in Fig. 6 (a), but all coefficients are 0.25 times smaller. The resulting distance in Fig. 6 (b) is shorter than that in Fig. 6 (a). Fig. 7 (b) and Fig. 8 (b) are illustrations of the distance but the coefficients are 0.25 times smaller than those in Fig. 7 (a) and Fig. 8 (b). This distance measure in (6) has a minimum distance, zero, when a, b, and f are all zeros. So we have to normalize parameters b and a. The coefficients are normalized by $\sqrt{|ab|}$ so that $|ab| = 1$. This is similar to [8] where the pattern is in the form $\mathbf{x}^T\mathbf{A}\mathbf{x} = r^2$ and in order to reflect r in the distance, $\mathbf{A}$ is normalized to $||\det(\mathbf{A})|| = 1$. Comparing this with (1), $\mathbf{A} = \begin{bmatrix} a & 0 \\ 0 & b \end{bmatrix}$, $||\det(\mathbf{A})|| = 1$ implies $|ab| = 1$.

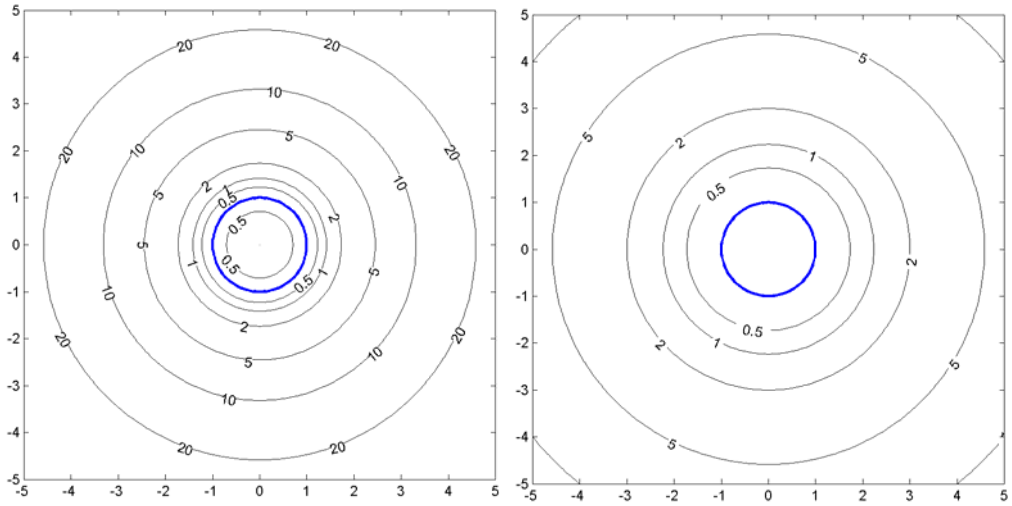

(a) (b)

Fig. 6. (a) Distance from points to the circle $x^2 + y^2 = 1$. (b) Distance from points to the circle $0.25x^2 + 0.25\, y^2 = 0.25$

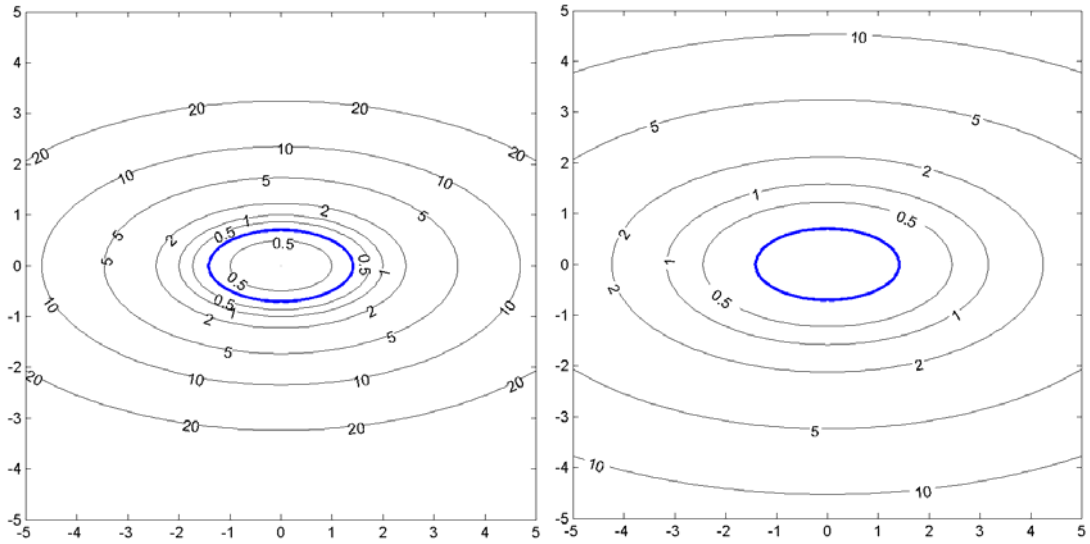

(a) (b)

Fig. 7. (a) Distance from points to the ellipse $0.5x^2 + 2y^2 = 1$. (b) Distance from points to the ellipse $0.125x^2 + 0.5y^2 = 0.25$.

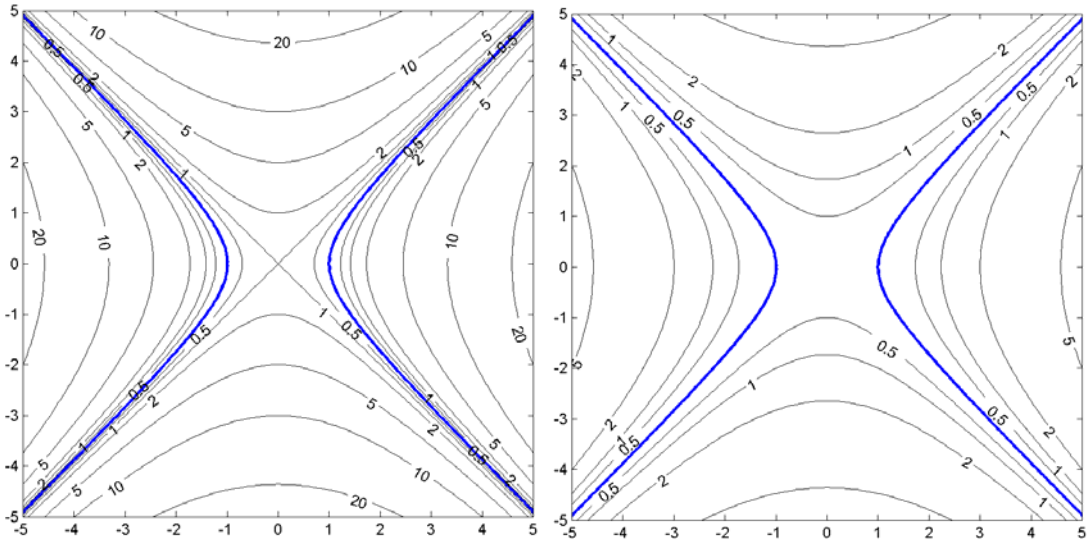

(a) (b)

Fig. 8. (a) Distance from points to the hyperbola $x^2 - y^2 = 1$. (b) Distance from points to the hyperbola $0.25x^2 - 0.25y^2 = 0.25$.

3.1.3 Distance from a point to *K* patterns

Error or distance from a point to the patterns is defined as the geometric mean of the distances from the point to all patterns. The error of the *i*th point $\mathbf{x}_i$ is

$$E_i = E(\mathbf{x}_i) = \left[d_1(\mathbf{x}_i)d_2(\mathbf{x}_i)...d_k(\mathbf{x}_i)...d_K(\mathbf{x}_i)\right]^{\frac{1}{K}}, \tag{7}$$

where K is the total number of patterns. If the point is on any pattern, the error of this point will be zero. Fig. 9 shows the error of a point to all patterns. The distance layer computes the distance from a point to each pattern by (6), and the error layer outputs the error from a point to all patterns by (7).

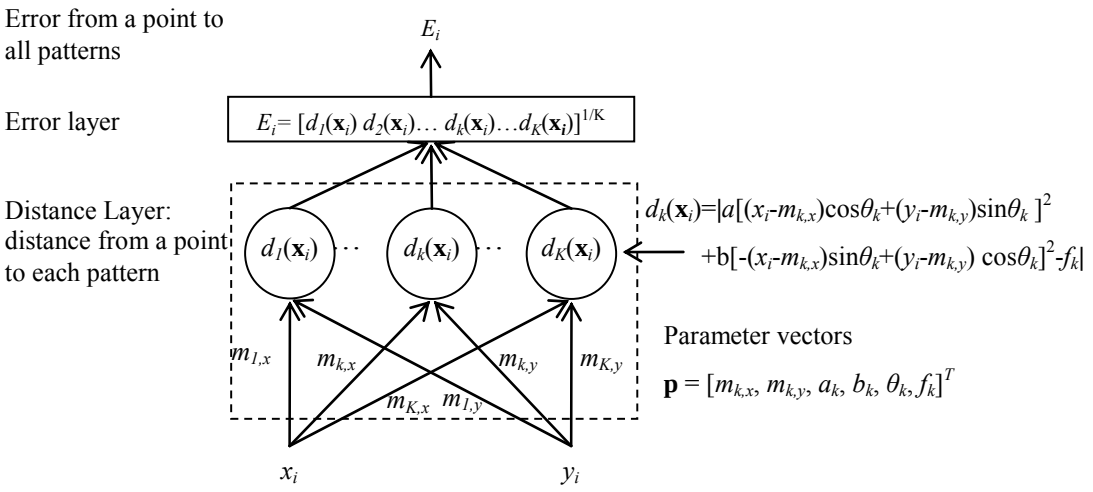

Fig. 9. Distance from a point to all patterns. *i* is the index of the input point. *k* is the index of the pattern, and *K* is the number of patterns.

3.1.4 Error from *N* input data to *K* patterns in the system

Fig. 10 illustrates the error or energy of the system from *N* input points to *K* patterns. The error or energy of the system is defined as the average of the error of points,

$$E = \frac{1}{N}\sum_{i=1}^{N} E_i \ . \tag{8}$$

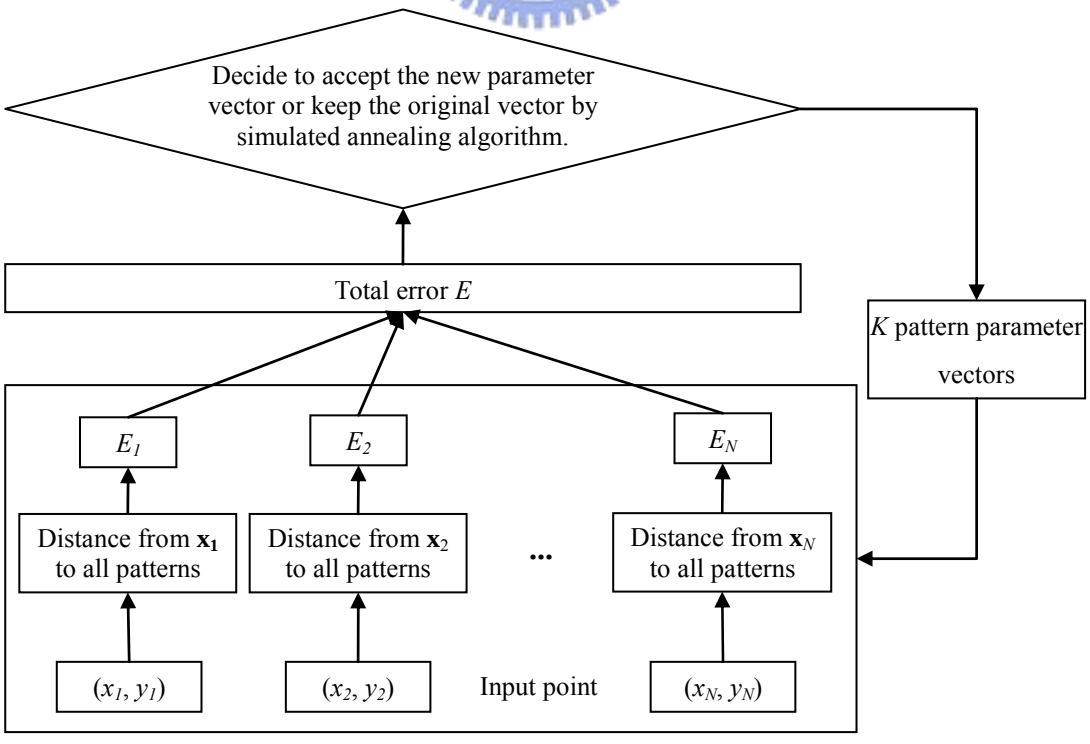

Fig. 10. Total error of the system and procedure of simulated annealing.

3.2 *Simulated annealing parameter detection system*

We use SA to detect the parameter vector of each pattern. Our goal is to find a set of parameter vectors that can globally minimize the error of the system. Using the temperature decreasing function $T(t)$

$$T(t) = T_{\max} \times 0.98^{(t-1)} \qquad \text{for } t = 1, 2, 3, \ldots \tag{9}$$

as in [10].

Adjusting all parameters at one time is not efficient in convergence [8]. We use four steps in adjusting parameters also. The adjusting order is the center **(**m_x, m_y), the major and minor axes, b and a, and then the rotation angle θ, followed by the size r. The followings is algorithm to detect ellipses, hyperbolas, and lines. Here, lines are considered as the asymptotes of hyperbolas.

3.2.1 Simulated annealing algorithm for parameter detection

This algorithm is the general algorithm to detect ellipses, hyperbolas, and it treats lines as asymptotes of hyperbolas. Also, from Table 1, the change of the signs of a, b, and f simultaneously makes the same patterns. So we have the constraint $f \geq 0$ in the algorithm.

Algorithm: SA algorithm to detect parameter vectors of K patterns including ellipses, circles, hyperbolas, and lines as asymptotes.
Input: N points in an image. Set K as the number of patterns.
Output: A set of detected K parameter vectors.

Step 1: Initialization.

In the initial step $t = 1$, choose $T(1) = T_{\max}$ at high temperature, and define the temperature decreasing function as in (9), $T(t) = T_{\max} \times 0.98^{(t-1)}$

Initialize parameter vectors $\mathbf{p}_1, \mathbf{p}_2, \ldots, \mathbf{p}_k, \ldots, \mathbf{p}_K$, where $\mathbf{p}_k = [m_{x,k}, m_{y,k}, a_k, b_k, \theta_k, f_k]^T$, one $\mathbf{p}$ is for one pattern, and set $\mathbf{P} = (\mathbf{p}_1, \mathbf{p}_2, \ldots, \mathbf{p}_k, \ldots, \mathbf{p}_K)$.

Calculate energy $E(\mathbf{P})$ as (6), (7), and (8).

Step 2: Randomly change parameter vectors and decide the new parameter vectors in the same temperature.

For $m = 1$ to Nt (Nt trials in a temperature)

For $k = 1$ to K (k is the index of the pattern)

Start a trial, including (a), (b), (c), and (d) in the following.

(a) Randomly change the center of the kth pattern:

$$[m'_{k,x} \;\; m'_{k,y}]^T = [m_{k,x} \; m_{k,y}]^T + \alpha_m \mathbf{n}, \tag{10}$$

where $\mathbf{n} = [n_1 \; n_2]^T$ is a 2×1 random vector, n_1 and n_2 are Gaussian random variables with $N(0, 1)$ and α_m is a constant. Now, $\mathbf{p}'_k = [m'_{k,x}, m'_{k,y}, a_k, b_k, \theta_k, r_k]^T$, and $\mathbf{P}' = (\mathbf{p}_1, \mathbf{p}_2, \ldots, \mathbf{p}'_k, \ldots, \mathbf{p}_K)$.
Calculate the new energy $E(\mathbf{P}')$ from N points to K patterns. Using Metropolis criterion decides whether or not to accept $\mathbf{P}'$: If the new energy is less than or equal to the original one, $\Delta E = E(\mathbf{P}') - E(\mathbf{P}) \leq 0$, accept $\mathbf{P}'$. Otherwise, the new energy is higher than the original one, $\Delta E = E(\mathbf{P}') - E(\mathbf{P}) > 0$. In this case, it computes $prob = \exp[-\Delta E/T(t)]$, and generates a random number x uniformly distributed over (0, 1). If $prob \geq x$, accept $\mathbf{P}'$; otherwise, reject it, and keep $\mathbf{P}$.

(b) Randomly change the shape parameters:

$$[a'_k \; b'_k] = [a_k \; b_k] + \alpha_{ab} \mathbf{n}, \tag{11}$$

and normalize it by $\sqrt{|a'_k \; b'_k|}$, where $\mathbf{n} = [n_1 \; n_2]^T$ is a 2×1 random vector, n_1 and n_2 are Gaussian random variables with $N(0, 1)$ and α_{ab} is a constant. Now, $\mathbf{p}'_k = [m_{k,x}, m_{k,y}, a'_k, b'_k, \theta_k, r_k]^T$, and $\mathbf{P}' = (\mathbf{p}_1, \mathbf{p}_2, \ldots, \mathbf{p}'_k, \ldots, \mathbf{p}_K)$.
Similar to Step 2(a), calculate the new energy $E(\mathbf{P}')$ from N points to K patterns. Using Metropolis criterion decides whether or not to accept $\mathbf{P}'$.

(c) Randomly change the angle:

$$\theta'_k = \theta_k + \alpha_\theta n, \tag{12}$$

where n is a Gaussian random variable with $N(0, 1)$ and α_θ is a constant. Here, the angle is in degree. Now, $\mathbf{p}'_k = [m_{k,x}, m_{k,y}, a_k, b_k, \theta'_k, r_k]^T$, and $\mathbf{P}' = (\mathbf{p}_1, \mathbf{p}_2, \ldots, \mathbf{p}'_k, \ldots, \mathbf{p}_K)$.
Similar to Step 2(a), calculate the new energy $E(\mathbf{P}')$ from N points to K patterns. Using Metropolis criterion decides whether or not to accept $\mathbf{P}'$.

(d) Randomly change the size:

$$f'_k = |f_k + \alpha_f n|, \tag{13}$$

where n is a Gaussian random variable with $N(0, 1)$ and α_f is a constant. Now, $\mathbf{p}'_k = [m_{k,x}, m_{k,y}, a_k, b_k, \theta_k, f'_k]^T$, and $\mathbf{P}' = (\mathbf{p}_1, \mathbf{p}_2, \ldots, \mathbf{p}'_k, \ldots, \mathbf{p}_K)$.

Similar to Step 2(a), calculate the new energy $E(\mathbf{P}')$ from N points to K patterns. Using Metropolis criterion decides whether or not to accept $\mathbf{P}'$.

End for k

End for m

Step 3: Cool the System.

Decrease temperature T according to the cooling function (9), $T(t) = T_{\max} \times 0.98^{(t-1)}$, for $t = 1, 2, 3, \ldots$, and repeat Step 2, and 3 until the temperature is low enough, for examples, repeat 500 times.

3.2.2 Simulated annealing algorithm to detect North-South opening hyperbolas

For seismic applications, patterns of reflection wave are North-South opening hyperbolas. Besides, patterns of direct waves are asymptotes of hyperbolas [3]-[5]. Equation of a North-South opening hyperbola is

$$a(x - m_x)^2 + b(y - m_y)^2 = f \,. \tag{14}$$

with $a < 0$, $b > 0$, $f \geq 0$. So the parameters to be detected are $\mathbf{p} = [m_x, m_y, a, b, f]^T$ and the distance from a point to a pattern becomes

$$d_k(x_i, y_i) = | a(x_i - m_{k,x})^2 + b(y_i - m_{k,y})^2 - f_k | \,. \tag{15}$$

We consider these properties and modify the algorithm to be just for North-South opening hyperbolas. This algorithm proves the detected patterns have the properties of North-South opening hyperbolas.

Algorithm: SA algorithm to detect parameter vectors of K North-South opening hyperbolas.

Input: N points in an image. Set K as the number of patterns.

Output: A set of detected K parameter vectors.

Step 1: Initialization.

In the initial step $t = 1$, choose $T(1) = T_{\max}$ at a high temperature, and define the temperature decreasing function as in (9), $T(t) = T_{\max} \times 0.98^{(t-1)}$.

Initialize parameter vectors $\mathbf{p}_1, \mathbf{p}_2, \ldots, \mathbf{p}_k, \ldots, \mathbf{p}_K$, where $\mathbf{p}_k = [m_{k,x}, m_{k,y}, a_k, b_k, f_k]^T$, one $\mathbf{p}$ is for one North-South opening hyperbola, and set $\mathbf{P} = (\mathbf{p}_1, \mathbf{p}_2, \ldots, \mathbf{p}_k, \ldots, \mathbf{p}_K)$.

Calculate energy $E(\mathbf{P})$ as (15), (7), and (8).

Step 2: Randomly change parameter vectors and decide the new parameter vectors in the same temperature.

For m = 1 to Nt (Nt trials in a temperature)

For k = 1 to K (k is the index of the pattern)

Start a trial, including (a), (b), and (c) in the following.

(a) Randomly change the center of the kth pattern:

$$[m'_{k,x} \;\; m'_{k,y}]^T = [m_{k,x} \; m_{k,y}]^T + \alpha_m \mathbf{n}, \tag{16}$$

where $\mathbf{n} = [n_1 \; n_2]^T$ is a 2 × 1 random vector, n_1 and n_2 are Gaussian random variables with $N(0, 1)$ and α_m is a constant. Now, $\mathbf{p}'_k = [m'_{k,x}, m'_{k,y}, a_k, b_k, f_k]^T$, and $\mathbf{P}' = (\mathbf{p}_1, \mathbf{p}_2, \ldots, \mathbf{p}'_k, \ldots, \mathbf{p}_K)$.

Calculate the new energy $E(\mathbf{P}')$ from N points to K patterns. Using Metropolis criterion decides whether or not to accept $\mathbf{P}'$: for the new energy less than or equal to the original one, $\Delta E = E(\mathbf{P}') - E(\mathbf{P}) \leq 0$, accept $\mathbf{P}'$. Otherwise, new energy is higher than the original one, $\Delta E = E(\mathbf{P}') - E(\mathbf{P}) > 0$. In this case, compute $prob = \exp[-\Delta E/T(t)]$, and generate a random number x uniformly distributed over (0, 1). If $prob \geq x$, accept $\mathbf{P}'$; otherwise, reject it, and keep $\mathbf{P}$.

(b) Randomly change the shape parameters:

$$[a'_k \; b'_k] = [a_k \; b_k] + \alpha_{ab} \mathbf{n} \tag{17}$$

and normalize it by $\sqrt{|a'_k \, b'_k|}$, where $\mathbf{n} = [n_1 \; n_2]^T$ is a 2 × 1 random vector, n_1 and n_2 are Gaussian random variables with $N(0, 1)$ and α_{ab} is a constant. If $a'_k > 0$ or $b'_k < 0$, regenerate a_k and b_k. Now, $\mathbf{p}'_k = [m_{k,x}, m_{k,y}, a'_k, b'_k, f_k]^T$, and $\mathbf{P}' = (\mathbf{p}_1, \mathbf{p}_2, \ldots, \mathbf{p}'_k, \ldots, \mathbf{p}_K)$.

Similar to Step 2(a), calculate the new energy $E(\mathbf{P}')$ from N points to K patterns. Using Metropolis criterion decides whether or not to accept $\mathbf{P}'$.

(c) Randomly change the size:

$$f'_k = | f_k + \alpha_f n |, \tag{18}$$

Where n is a Gaussian random variable with $N(0, 1)$ and α_f is a constant. Now, $\mathbf{p}'_k = [m_{k,x}, m_{k,y}, a_k, b_k, f'_k]^T$, and $\mathbf{P}' = (\mathbf{p}_1, \mathbf{p}_2, \ldots, \mathbf{p}'_k, \ldots, \mathbf{p}_K)$.

Similar to Step 2(a), calculate the new energy $E(\mathbf{P}')$ from N points to K patterns. Using Metropolis criterion decides whether or not to accept $\mathbf{P}'$.

End for k

End for m

Step 3: Cool the System.

Decrease temperature T according to the cooling function (9), $T(t)= T_{\max}\times 0.98^{(t-1)}$, for t = 1, 2, 3, …, and repeat Step 2, and 3 until the temperature is low enough, for examples, repeat 500 times.

Fig. 11 - Fig. 14 illustrate a possible procedure of SA algorithm. The example has some points on an ellipse. There is only one pattern K = 1, so $\mathbf{P} = \mathbf{p}_1$. Fig. 11 shows the trial of the center.

In the step 1, at a certain temperature, the center (m_x, m_y) is randomly displaced to (m'_x, m'_y), and the parameter vector changes from $\mathbf{P} = \mathbf{p}_1 = [m_{1,x}, m_{1,y}, a_1, b_1, f_1]^T$ to $\mathbf{P}' = \mathbf{p}_1' = [m'_{1,x}, m'_{1,y}, a_1, b_1, \theta_1, f_1]^T$. The resulting energy $E(\mathbf{P}')$ is less than the original energy $E(\mathbf{P})$. In this case, the trial parameter vector is accepted and set it as the starting parameter vector in the step 2, $\mathbf{P} \leftarrow \mathbf{P}' = \mathbf{p}_1' = [m'_{1,x}, m'_{1,y}, a_1, b_1, \theta_1, f_1]^T$.

Fig. 11. A trial of the center (m_x, m_y). (a): original parameter. (b): trial parameter. (c): preserved parameter.

In the step 2, as shown in Fig. 12, the shape parameters b and a are randomly changed to b' and a', and the parameter vector $\mathbf{p}_1$ becomes $\mathbf{p}_1'$, and this results in the energy $E(\mathbf{P}') > E(\mathbf{P})$. In this case, Metropolis criterion decides whether or not to accept the trial parameter by comparing $prob = \exp[-\Delta E/T(t)]$ and random number x. Assuming $prob \geq x$, the trial parameter vector with a higher energy is still preserved and set it as starting parameter vector in step 3, $\mathbf{P} \leftarrow \mathbf{P}' = \mathbf{p}_1' = [m_{1,x}, m_{1,y}, a'_1, b'_1, \theta_1, f_1]^T$.

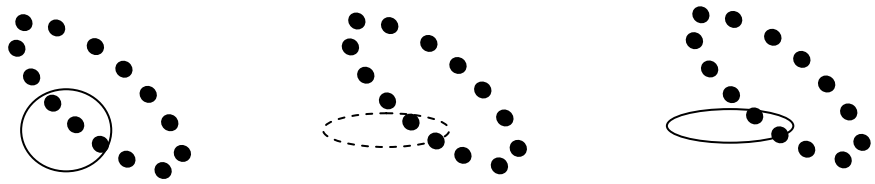

$E(\mathbf{P})$ $E(\mathbf{P}')$ $\Delta E = E(\mathbf{P}') - E(\mathbf{P}) > 0$

$prob = \exp[-\Delta E/T(t)] \geq r$

Accept $\mathbf{P}'$

(a) (b) (c)

Fig. 12. A trial of shape parameters b and a. (a): original parameter. (b): trial parameter. (c): preserved parameter.

In the step 3, the trial of the rotation angle gives the trial parameter vector $\mathbf{P}' = [m_{1,x}, m_{1,y}, a_1, b_1, \theta'_1, f_1]^T$, and the resulting energy $E(\mathbf{P}') < E(\mathbf{P})$. The trial parameter vectors is preserved and set as the starting parameter vector in the step 4, $\mathbf{P} \leftarrow \mathbf{P}'$. Fig. 13 illustrates the step 3.

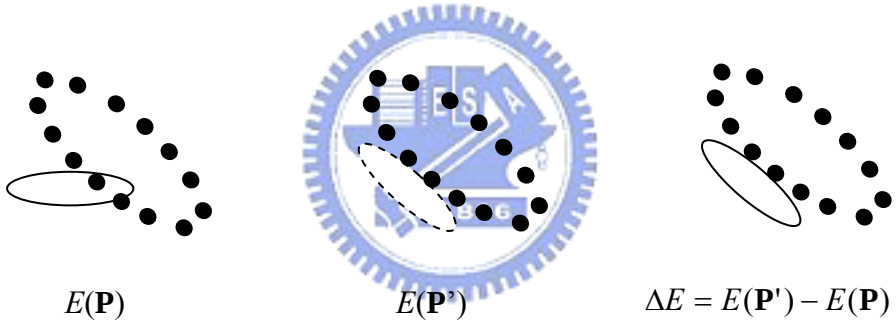

$E(\mathbf{P})$ $E(\mathbf{P}')$ $\Delta E = E(\mathbf{P}') - E(\mathbf{P}) < 0$

Accept $\mathbf{P}'$

(a) (b) (c)

Fig. 13. A trial of rotation angle θ. (a): original parameter. (b): trial parameter. (c): preserved parameter.

In the step 4, the trial of the size gives the trial parameter vector $\mathbf{P}' = [m_{1,x}, m_{1,y}, a_1, b_1, \theta_1, f'_1]^T$, and the resulting energy $E(\mathbf{P}') > E(\mathbf{P})$. Metropolis criterion decides the preserved parameter vector in the same way, and this time, $prob < x$, so the trial parameter vector $\mathbf{P}'$ is rejected. The starting parameter vector in the next step is still the original one, $\mathbf{P} \leftarrow \mathbf{P}$. Fig. 14 illustrates the step 4.

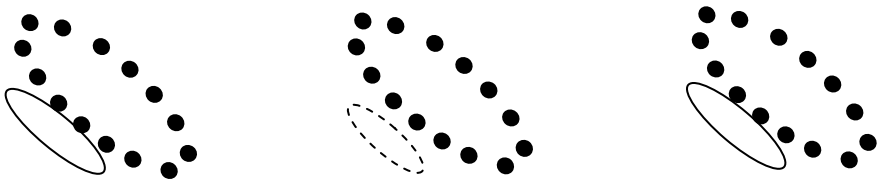

$E(\mathbf{P})$ $E(\mathbf{P}')$ $\Delta E = E(\mathbf{P}') - E(\mathbf{P}) > 0$

$prob=\exp[-\Delta E/T(t)] < r$

Reject $\mathbf{P}'$; keep $\mathbf{P}$

(a) (b) (c)

Fig. 14. A trial of *f*. (a): original parameter. (b): trial parameter. (c): preserved parameter.

Chapter 4

Implementation and Experimental Results

The experiments are first on simulated pattern detections in images with size 50 × 50. First, we use the general algorithm to detect hyperbolas, ellipses, and consider lines as asymptotes of hyperbolas. Then, we use the algorithm just for North-South opening hyperbolas. Experiments on determination of the number of patterns are also shown. In seismic applications, we detect line pattern of direct wave and hyperbolic pattern of reflection wave in the simulated and real seismic data.

4.1 *Detection of ellipses, hyperbolas, and lines*

The general algorithm can detect circles, ellipses, hyperbolas, and treats line as asymptote.

In initial stage, m_x and m_y are randomly distributed over (0, 50), $f_k = 0$, $a_k = 1$, $b_k = 1$, and $\theta_k = 0$. The cooling function is as (9) with a high enough temperature, $T_{\max} = 500$. We have 100 trials in the same temperature. The temperature decreases 500 times to $T = 0.0209$, and this temperature is low enough. Constants $\alpha_m = 1$, $\alpha_{ab} = 1$, $\alpha_\theta = 2$, and $\alpha_f = 2$.

Simulation 1: ellipses

Fig. 15 and Fig. 16 show the results of detecting ellipses. There are two ellipses in each figure and each ellipse has 50 points. Data are disturbed by Gaussian noise with zero mean and variance is 0.5, $N(0, 0.5) \times N(0, 0.5)$. The error vs. cooling cycles shows that the error oscillates at high temperature and goes toward lower energy and becomes stable as the temperature decreasing.

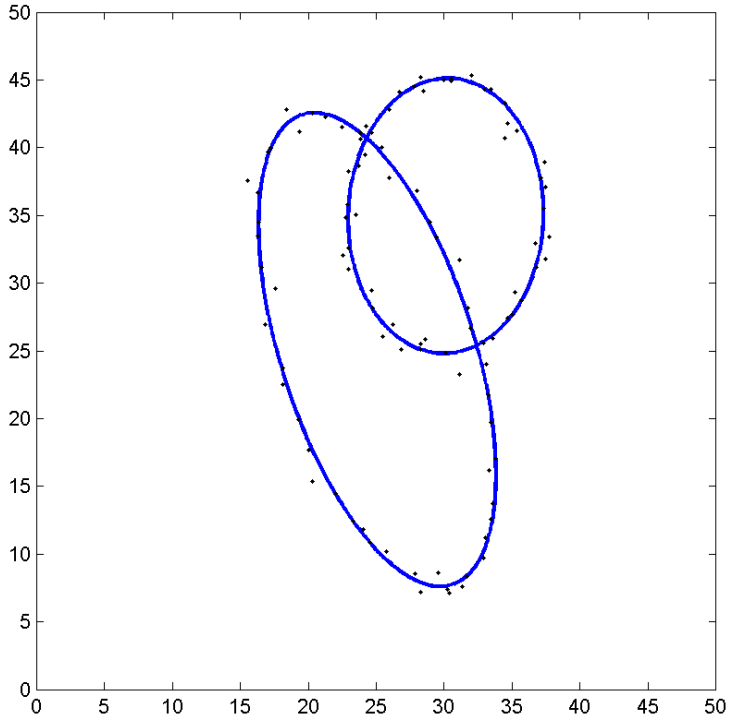

(a)

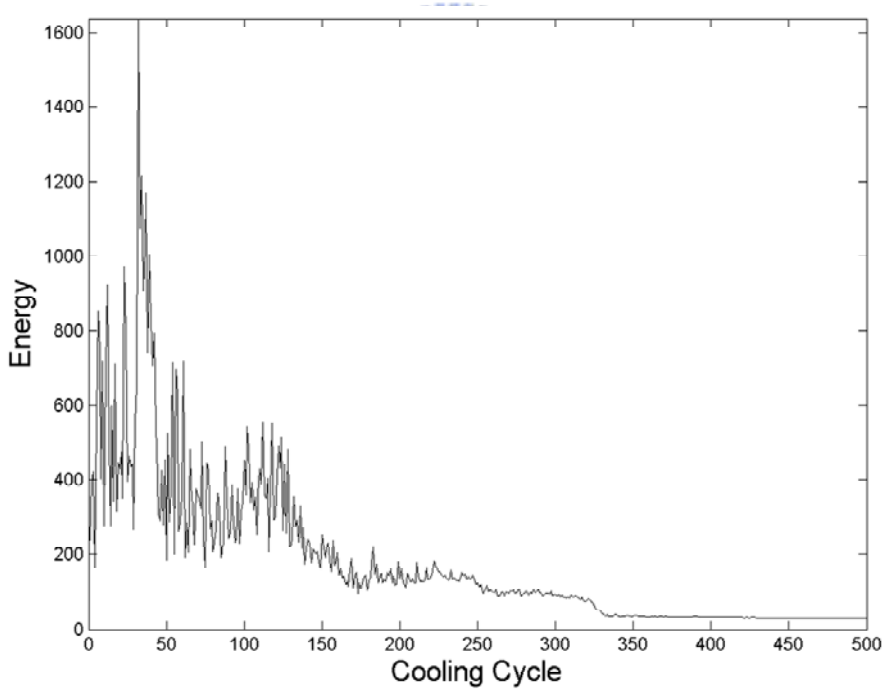

(b)

Fig. 15. Detection of ellipses – (a): 2 ellipses with noise. (b): error plot of (a) with cooling cycles.

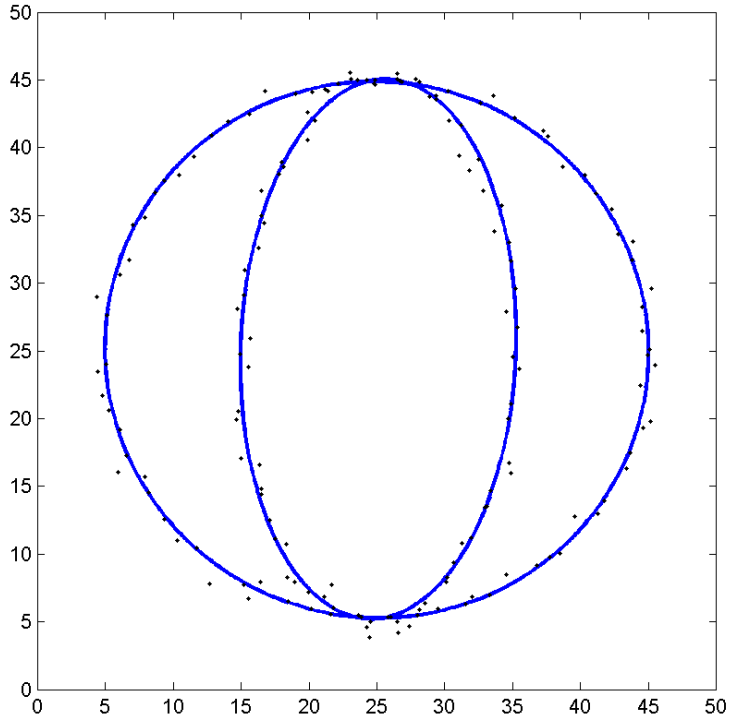

(a)

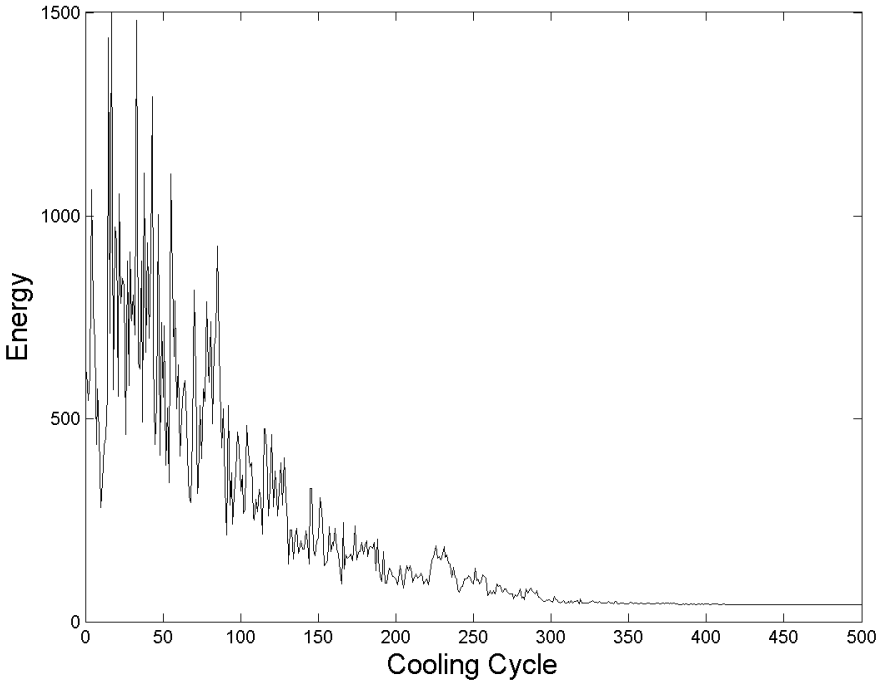

(b)

Fig. 16. Detection of ellipses – (a): 1 ellipse and 1 circle with noise. (b): error plot of (a) with cooling cycles.

Simulation 2: hyperbolas

Result of detecting hyperbolas are shown in Fig. 17 where $K = 2$. Patterns are with Gaussian noise $N(0, 0.5)\times N(0, 0.5)$. Figures of energy vs. cooling cycles are also shown.

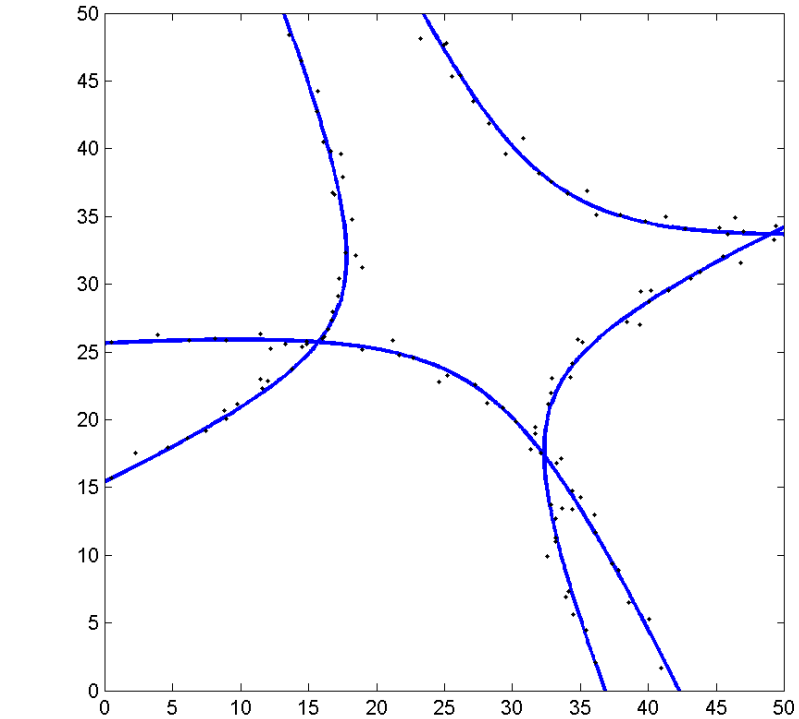

(a)

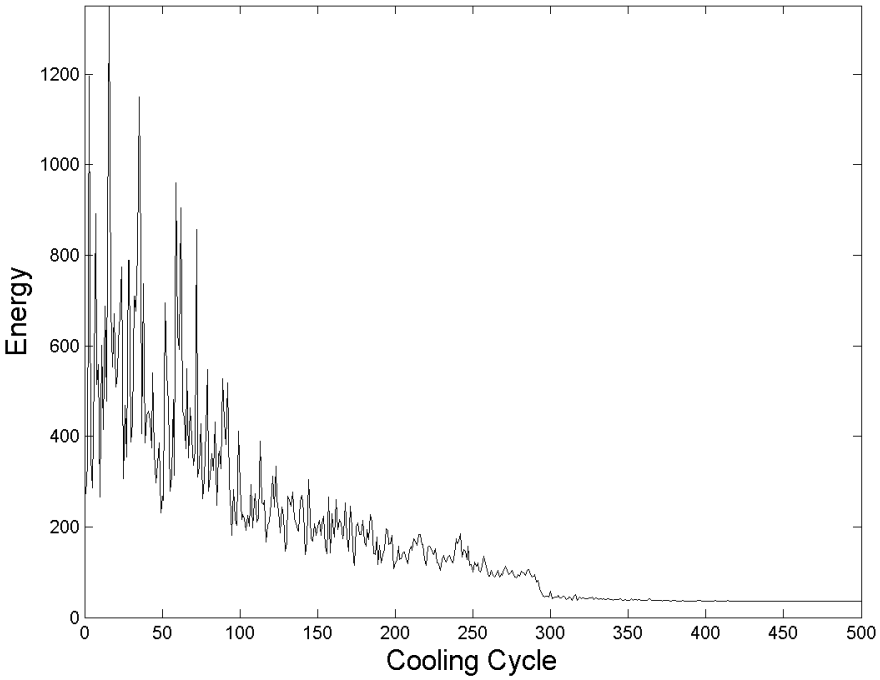

(b)

Fig. 17. Detection of hyperbolas − (a): 2 hyperbolas with noise. (b): error plot of (a) with cooling cycles.

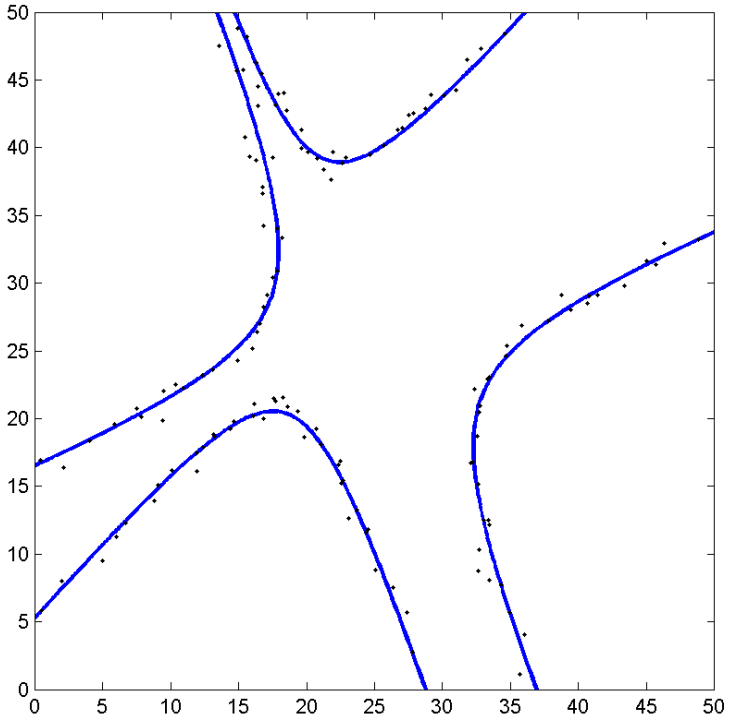

(a)

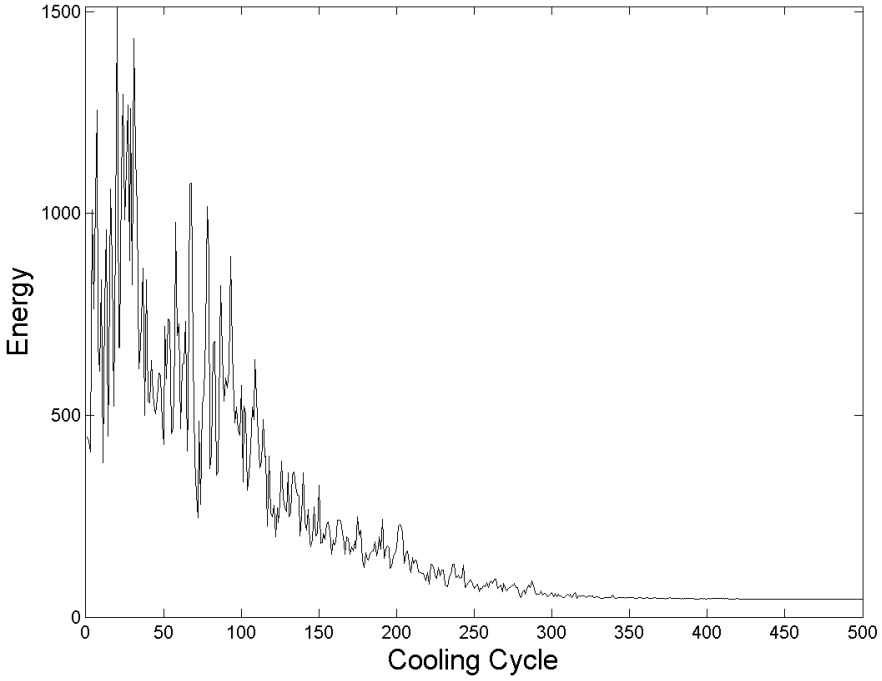

(b)

Fig. 18. Detection of hyperbolas − (a): 2 hyperbolas with noise. (b): error plot of (a) with cooling cycles.

Simulation 3: an ellipse and a hyperbola

Result of detecting ellipses and hyperbolas are shown in Fig. 19. Patterns are with Gaussian noise $N(0, 0.5) \times N(0, 0.5)$. Figures of energy vs. cooling cycles are also shown.

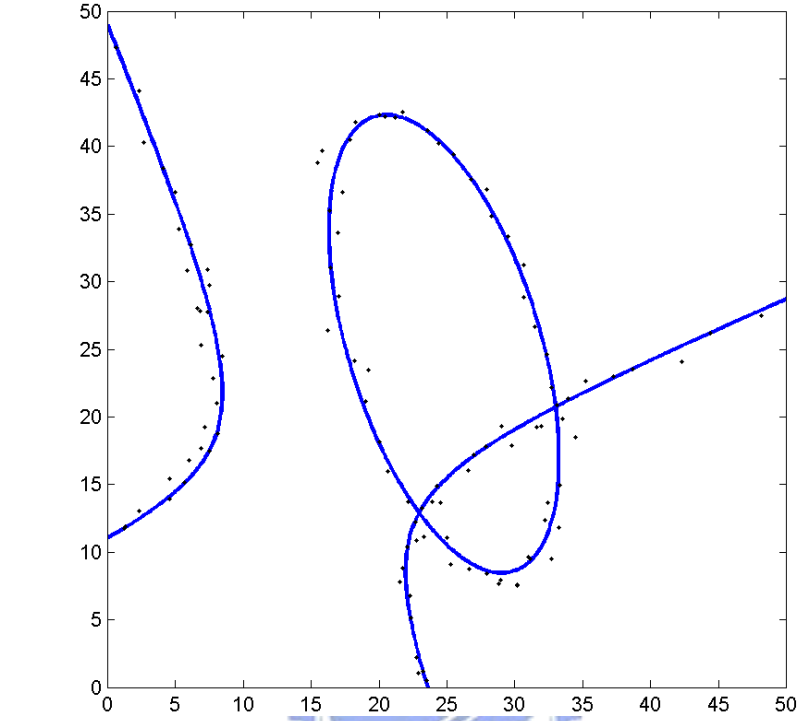

(a)

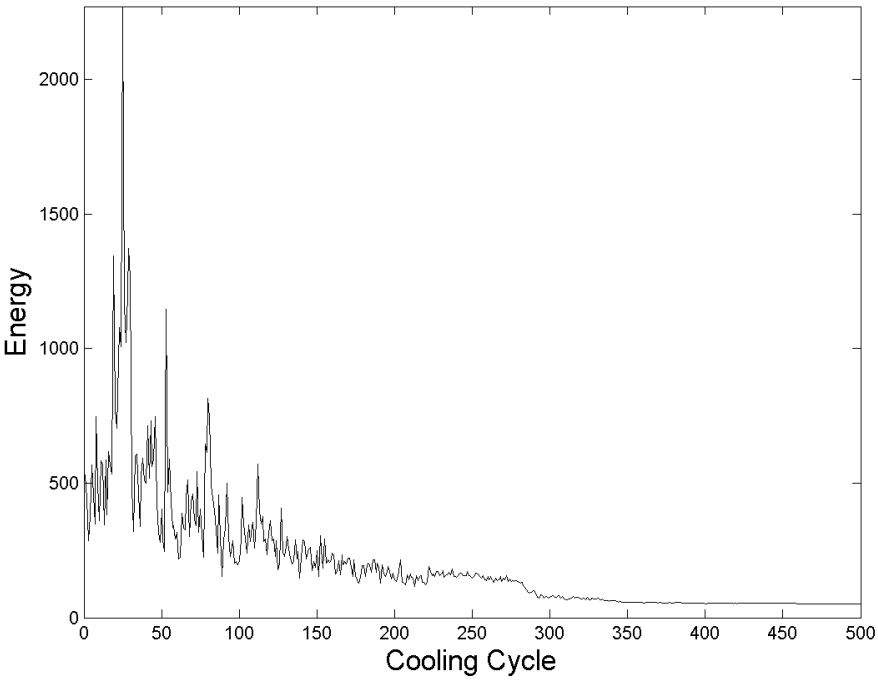

(b)

Fig. 19. Detection of ellipses and hyperbolas − (a): 1 ellipse and 1 hyperbola with noise. (b): error plot of (a) with cooling cycles.

Simulation 4: a line and an ellipse

Result of detecting ellipses and hyperbolas are shown in Fig. 20 where $K = 2$. Pattern are with Gaussian noise $N(0, 0.5) \times N(0, 0.5)$. Figures of energy vs. cooling cycles are also shown.

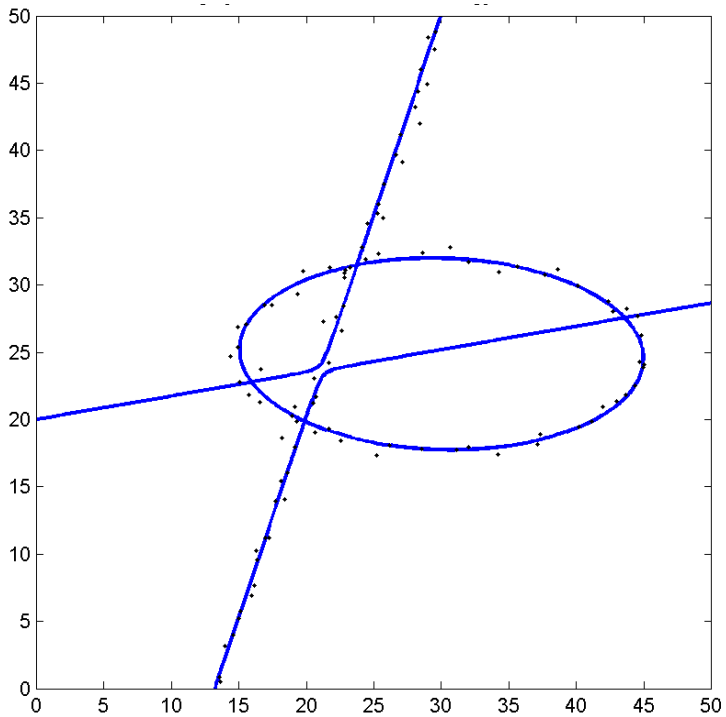

(a)

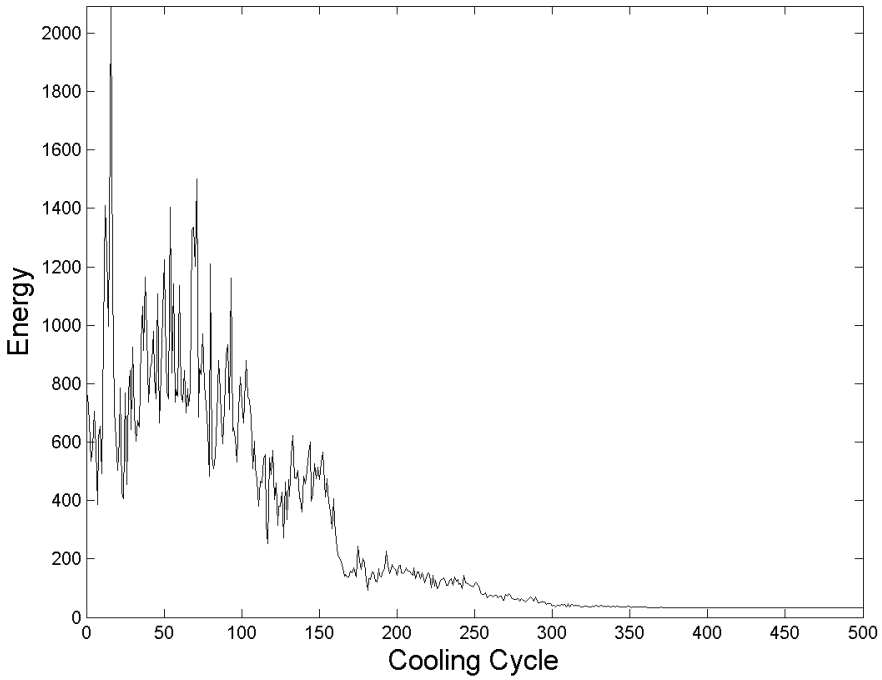

(b)

Fig. 20. Detection of ellipses and hyperbolas − (a): 1 ellipse and 1 hyperbola with noise. (b): error plot of (a) with cooling cycles.

Simulation 5: a line and a hyperbola

Result of detecting ellipses and hyperbolas are shown in Fig. 21 where K = 2. Patterns are with Gaussian noise $N(0, 0.5) \times N(0, 0.5)$. Figures of energy vs. cooling cycles are also shown.

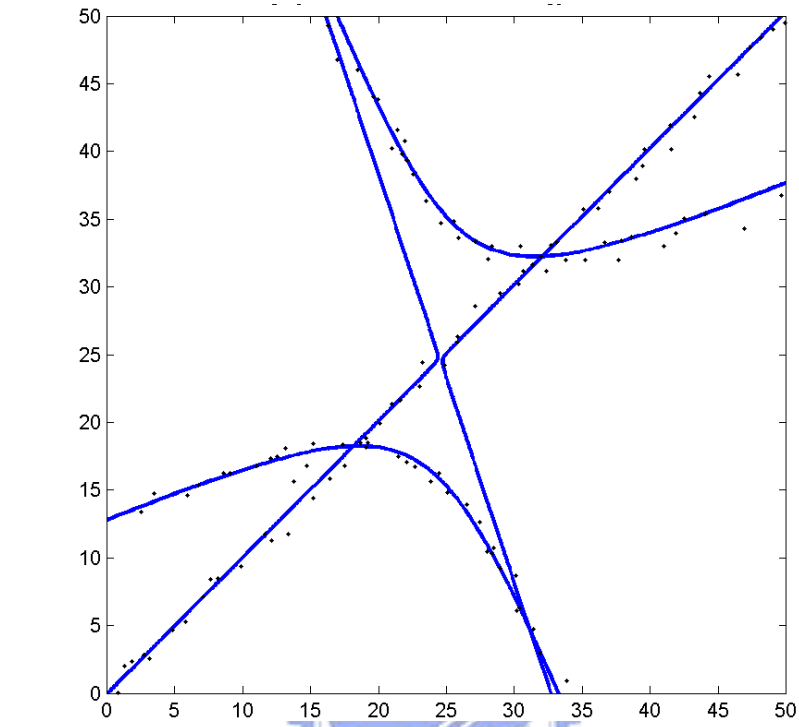

(a)

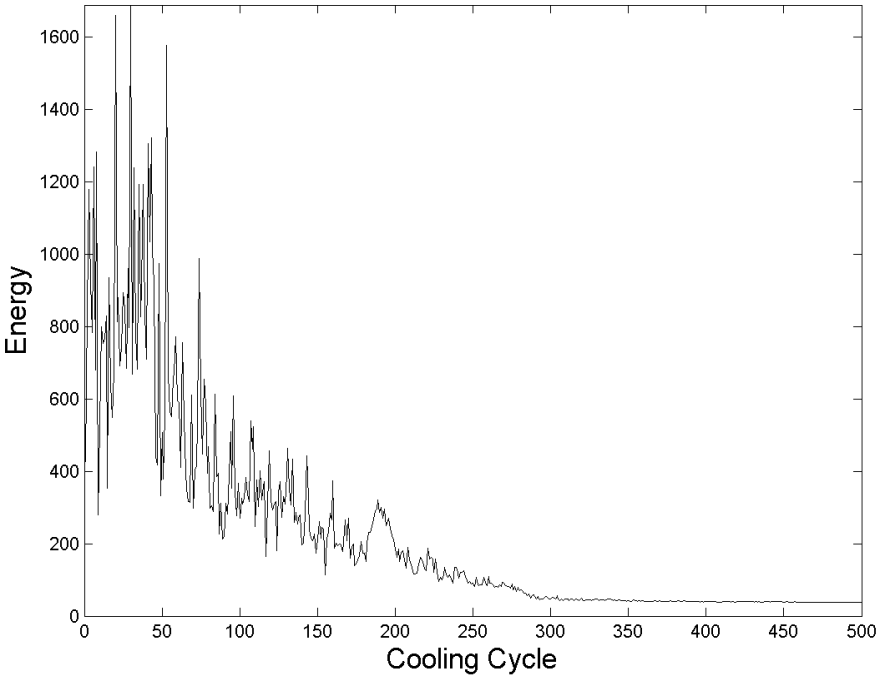

(b)

Fig. 21. Detection of line and hyperbola − (a): 1 line and 1 hyperbola with noise. (b): error plot of (a) with cooling cycles.

Simulation 6: two lines

Detected line patterns in Fig. 20 and Fig. 21 have parameter $f = 0.245$ and $f = 0.065$ respectively, but the ideal result is $f = 0$. To make detections more precise, we can put a constraint, $f = 0$, on detection of lines. Fig. 22 and Fig. 23 show the result of detecting lines data are also disturbed by Gaussian noise $N(0, 0.5)$. In Fig. 22, two lines are crossing at (0, 0). Since asymptotes of a hyperbola are two crossing lines, we can set $K = 1$ for Fig. 22. In Fig. 23, we set $K = 2$, so two additional lines appear.

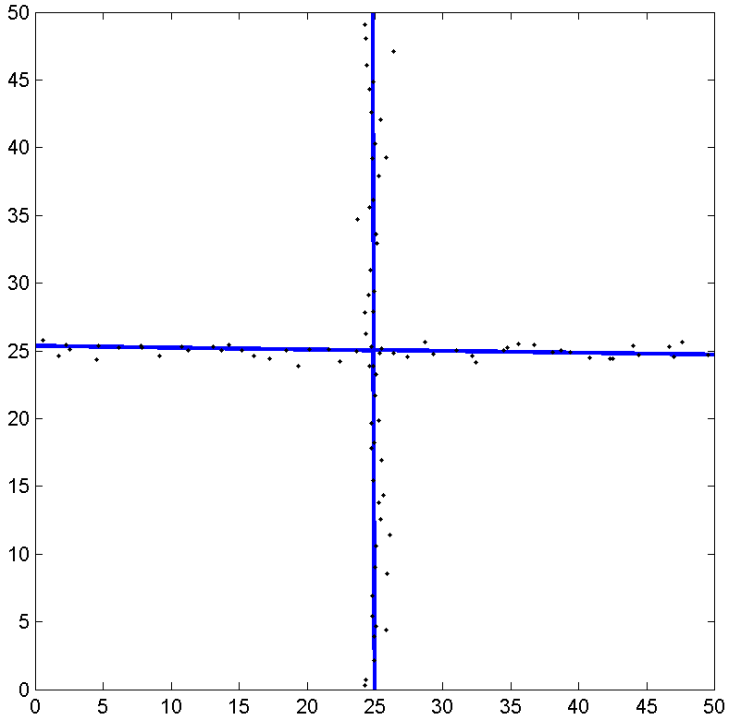

(a)

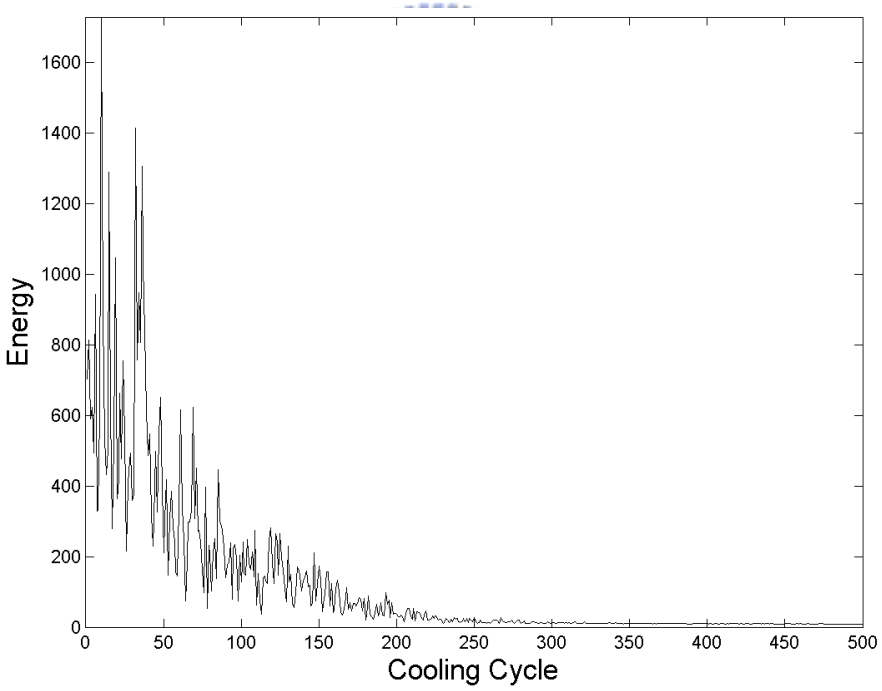

(b)

Fig. 22. Detection of lines by setting $f = 0 -$ (a): 2 lines with noise. (b): error plot of (a) with cooling cycles.

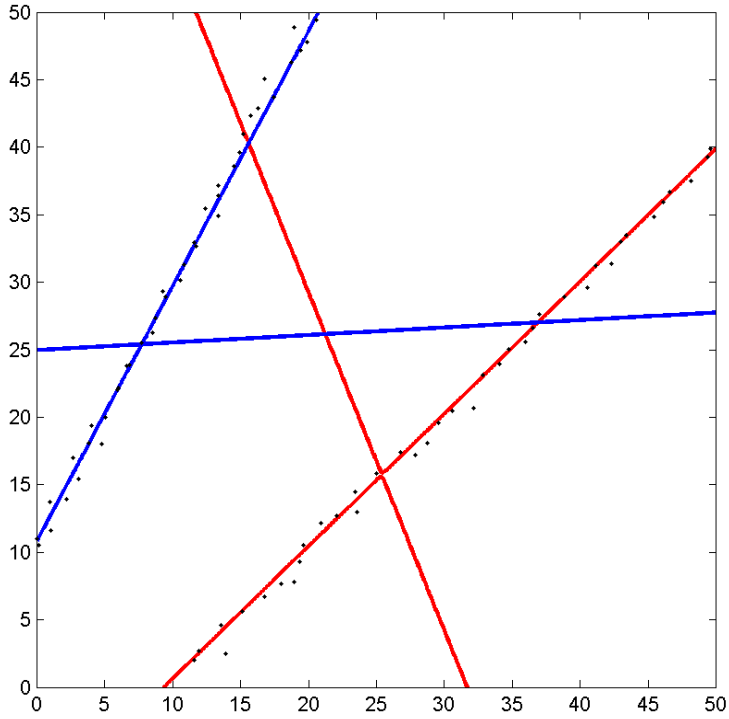

(a)

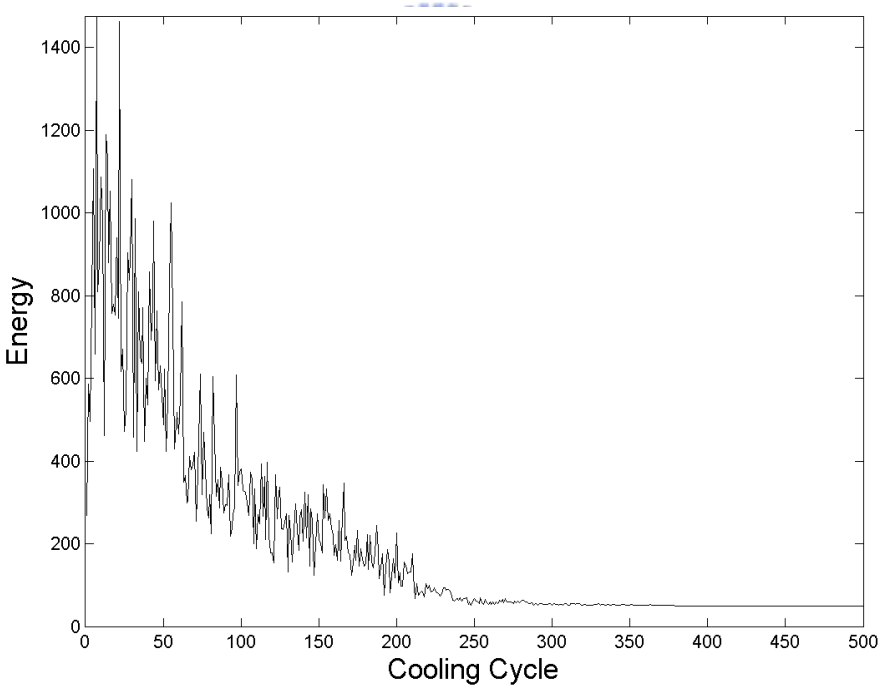

(b)

Fig. 23. Detection of lines by setting $f = 0 -$ (a): 2 lines with noise. (b): error plot of (a) with cooling cycles.

4.2 *Detection of North-South Opening Hyperbolas*

North-South opening hyperbolas have the properties $a < 0$, $b > 0$, and $\theta = 0$ in (5). We put these constraints in the algorithm to meet the properties. The algorithm used here is just for North-South opening hyperbola. The detected parameter vector $\mathbf{p}_k = [m_{k,x}, m_{k,y}, a_k, b_k, f_k]^T$.

In the initial step, $m_{k,x}$ and $m_{k,y}$ are randomly distributed over (0, 50), $a_k = -1$, $b_k = 1$, and $f_k = 0$ for hyperbolic pattern detection. The cooling function is as (9) with a high enough temperature, $T_{max} = 500$. We have 100 trials in the same temperature. The temperature decreases 500 times to $T = 0.0209$, and this temperature is low enough. Constants $\alpha_m = 1$, $\alpha_{ab} = 1$, and $\alpha_f = 2$.

Fig. 24 and Fig. 25 show the results of North-South opening hyperbolic pattern detection, where Fig. 24 (a) has 187 points and Fig. 25 (a) has 148 points. Each data is with Gaussian noise $N(0, 0.5) \times N(0, 0.5)$.

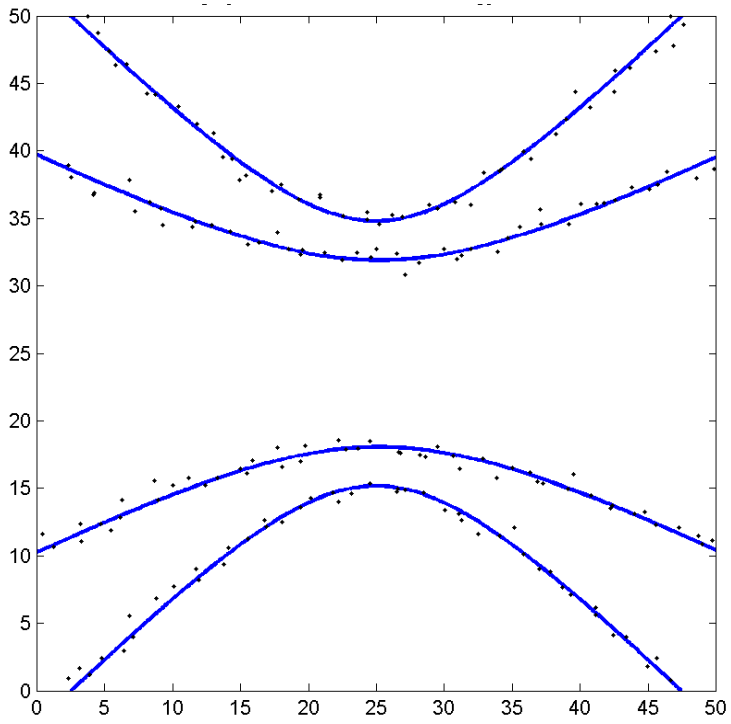

(a)

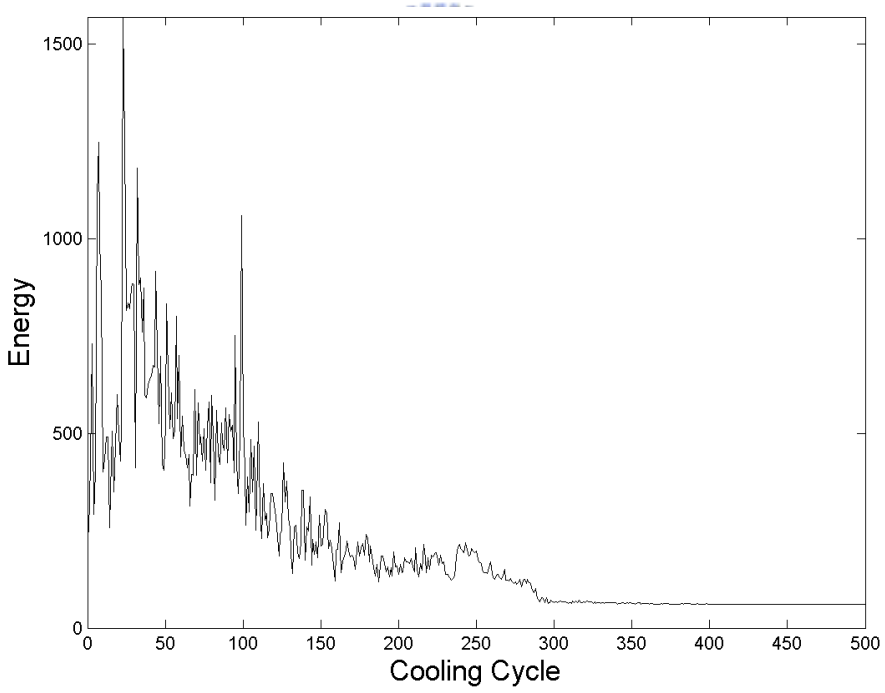

(b)

Fig. 24. Detection of hyperbolas − (a): 2 hyperbolas with noise. (b): Corresponding plot of error vs. cooling cycles of (a).

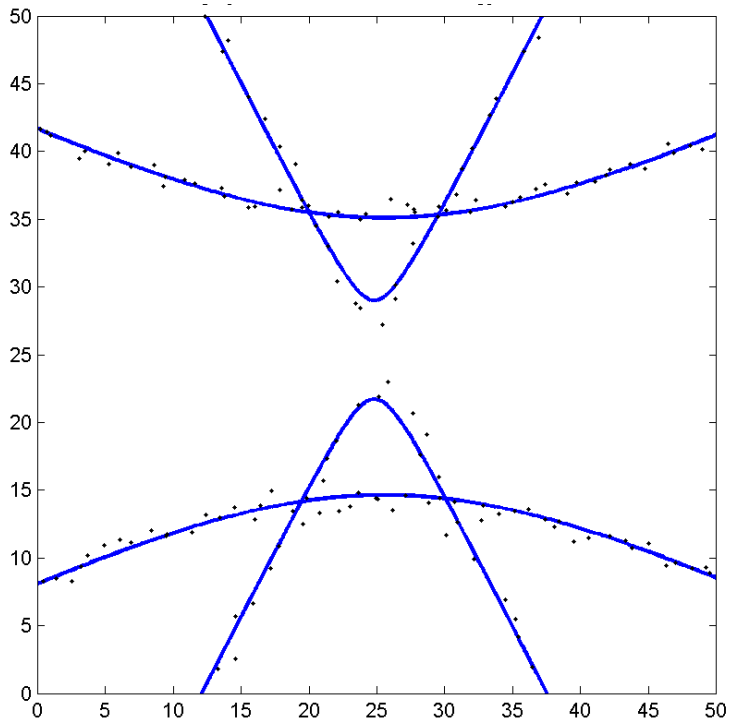

(a)

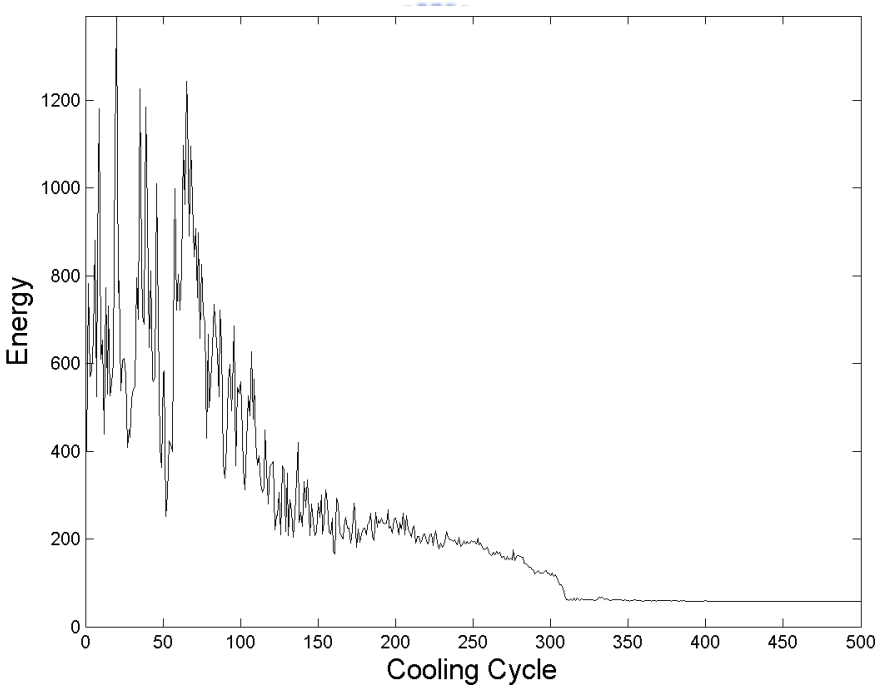

(b)

Fig. 25. Detection of hyperbolas − (a): 2 hyperbolas with noise. (b): Corresponding plot of error vs. cooling cycles of (a).

4.3 *Determination of the Number of Patterns*

In HTNN [8], the number of patterns was chosen by comparing the results from different number of patterns. Here we propose a method to determine the number of patterns, K, in the image. We define the detection error as

$$S = \frac{1}{N}\sum_{i=1}^{N} \min(d_1(\mathbf{x}_i), d_2(\mathbf{x}_i), ..., d_K(\mathbf{x}_i)), \tag{19}$$

where N is the number of input points. Equation (19) implies that the detection error is the average of the minimum distance from N points to their nearest patterns. Algorithm runs from pattern number K = 1, 2, …, until the detection error has a minimum and no improvement or lower than a threshold. At that time, the best choice of K is determined. Fig. 26 has three circles and shows the result of getting K automatically. In Fig. 26 (e), the detection error greatly decreases and no significant improvement after K = 3. So we choose K = 3. Table II lists the detection error in Fig. 26 (a)-(d).

The algorithm runs on Matlab 7.2 with Intel Duo Core CPU 1.66GHz and 1G RAM. Time consumption of SA algorithm is shown in Fig. 27. When K = 1, we have 6 dimensional parameter space and in the case of K = 2, that has 12 dimension. CPU time grows with the size of parameter space.

Table II

DETECTION ERROR IN Fig. 26

K	1	2	3	4	5
Detection error	218.9	49.2	7.50	7.21	7.20

Table III

CPU Time in Fig. 26

K	1	2	3	4	5
CPU time (seconds)	69.5	167.7	292.2	423.7	572.0

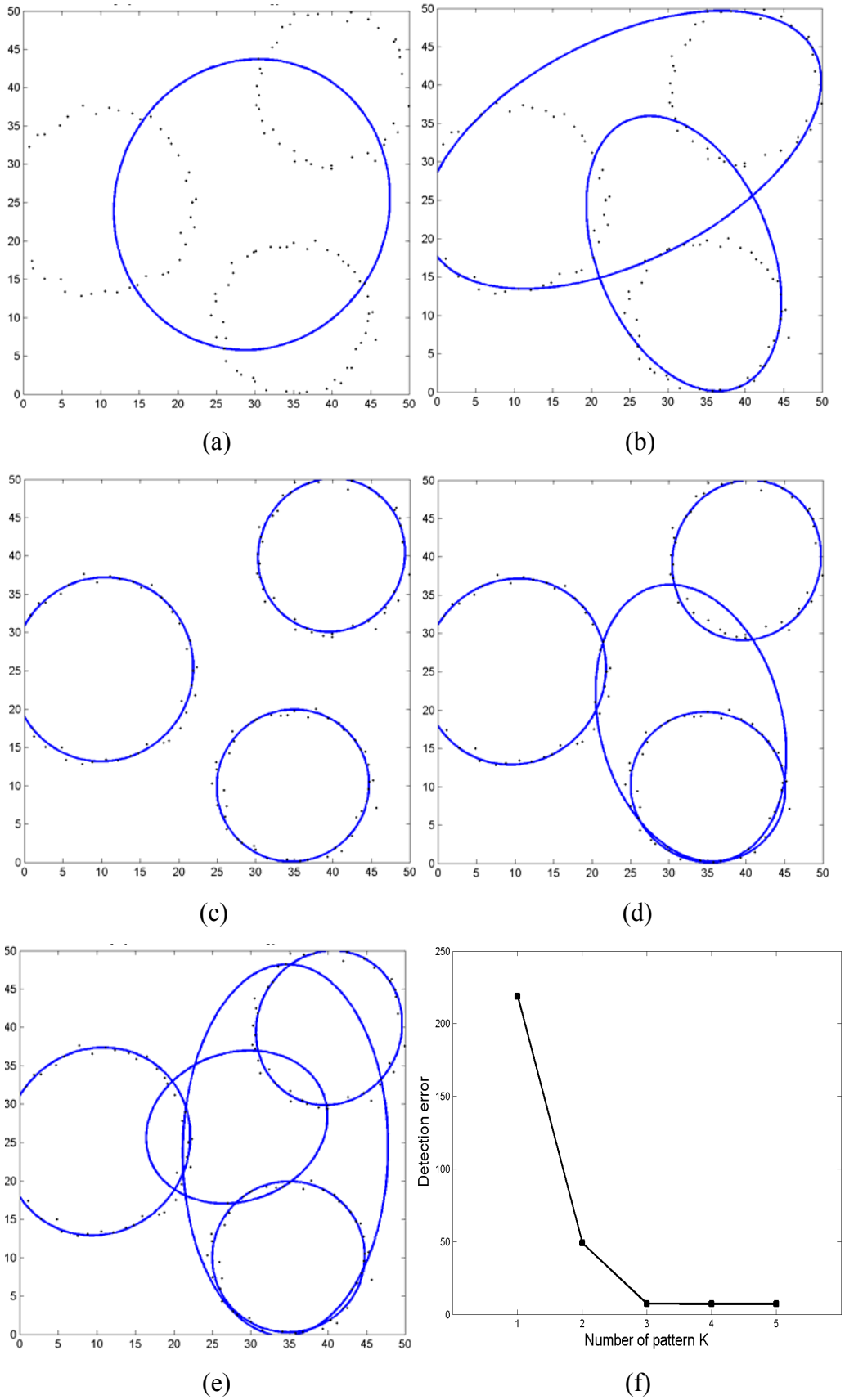

Fig. 26. Determination of number of patterns *K*. (a): *K*=1. (b): *K*=2. (c): *K*=3. (d): *K*=4. (e): *K*=5. (f): Detection error of (a), (b), (c), (d) and (e).

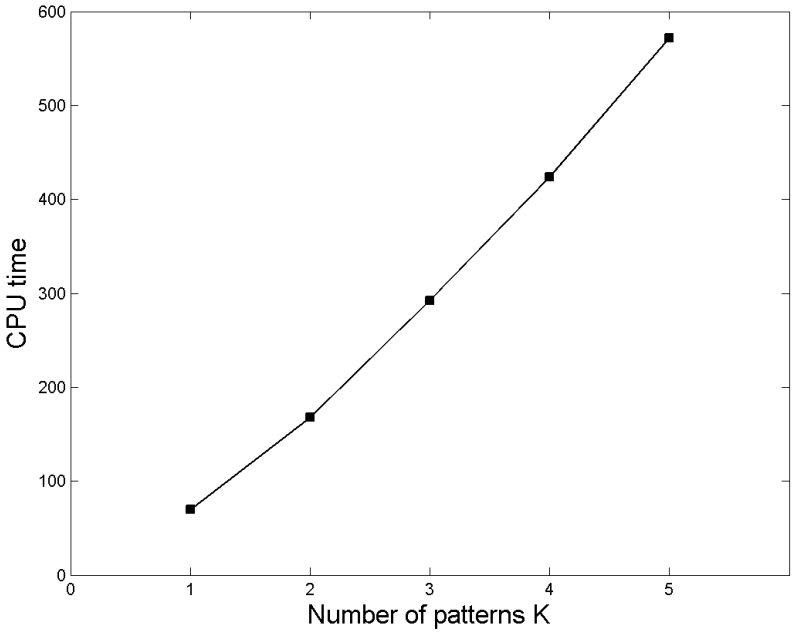

Fig. 27. CPU time (in seconds) vs. number of patterns *K*.

4.4 *Seismic Applications on Simulated data*

Experiments on simulated one-shot seismogram have two cases: horizontal reflection layer and dipping reflection layer. Two lines are the asymptote of the hyperbola [3]-[5], and the asymptote is a hyperbola with the same shape but size zero. So a line can be treated as a hyperbola. Here, we use the algorithm just for North-South opening hyperbolas.

Fig. 28 is the simulated horizontal reflection layer where the depth of the reflection layer is 500m and the velocity of the *p*-wave in the sedimentary rock is about 2,500m/sec [6]. There are 65 receiving stations on both side of explosion with 50m between each others. The sampling interval is 0.004 sec. The impulse response is 25 Hz Ricker wavelet. Reflection coefficient is 0.2 and noise is band-passed noise, 10.2539Hz ~ 59.5703Hz, with uniform distributed over (-0.2, 0.2).

Fig. 29 (a) shows a one-shot seismogram from horizontal reflection layer in Fig. 28. The horizontal axis in Fig. 29 is the trace number and the vertical axis stands for time t. The one-shot seismogram is first preprocessed by envelope processing in Fig. 29 (b) and thresholding [7] in Fig. 30 with the threshold 0.15. The image size is 512 × 65 where the origin is on the top-left corner with horizontal x-axis and vertical y-axis. The points are then used as the input to the parameter detection system.

The initial parameter $m_{k,x}$ and $m_{k,y}$ are random between 0 and 50, $a_k = -1$, $b_k = 1$, and $f_k = 1$. The cooling function is as (9) with a high enough temperature, $T_{\max} = 600$. There are $Nt = 100$ trials in a temperature. The temperature decreases 500 times. Constants $\alpha_m = 1$, $\alpha_{ab} = 0.5$, and $\alpha_f = 5$. Since lines of direct wave is asymptotes of a hyperbola, we set $f_1 = 0$. The result and the error plot are shown in Fig. 31 (a) and (b).

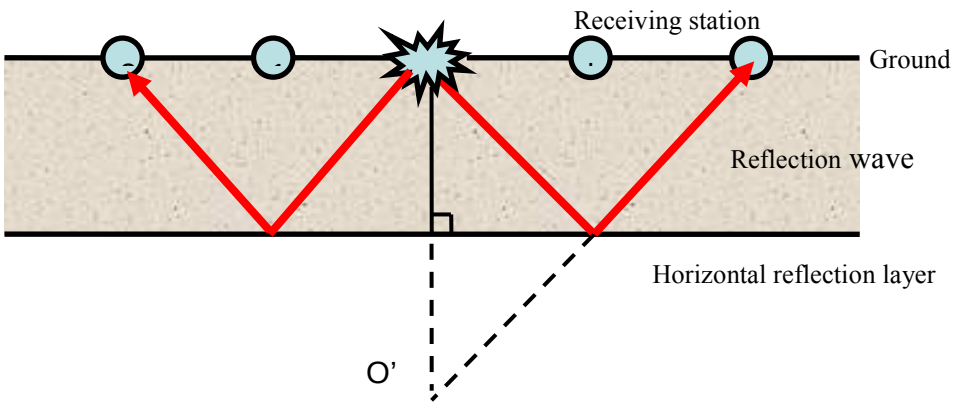

Fig. 28. Illustration of horizontal reflection layer.

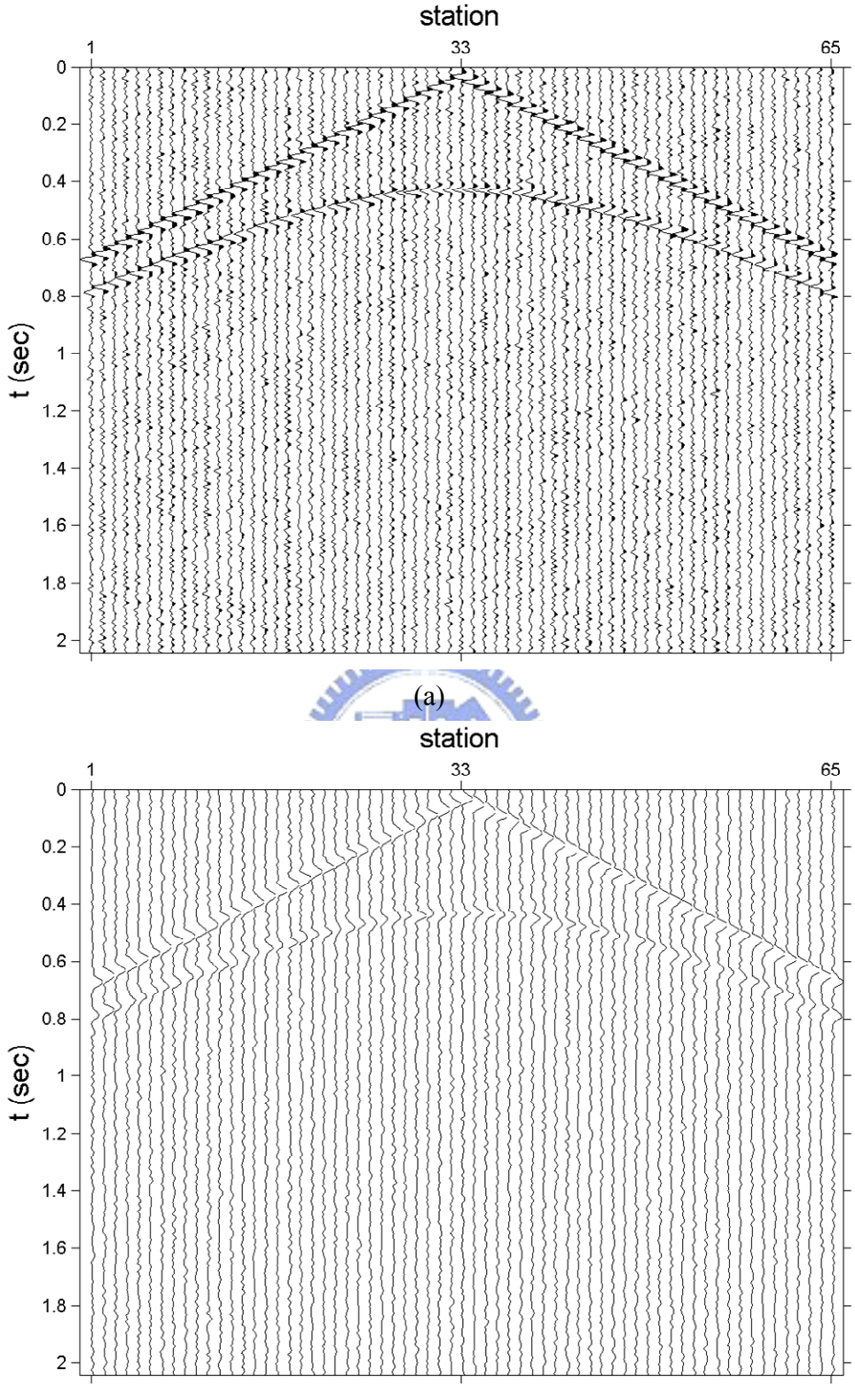

Fig. 29. Simulated seismic patterns − (a): Simulated one-shot seismogram (horizontal reflection layer). (b): After envelope processing.

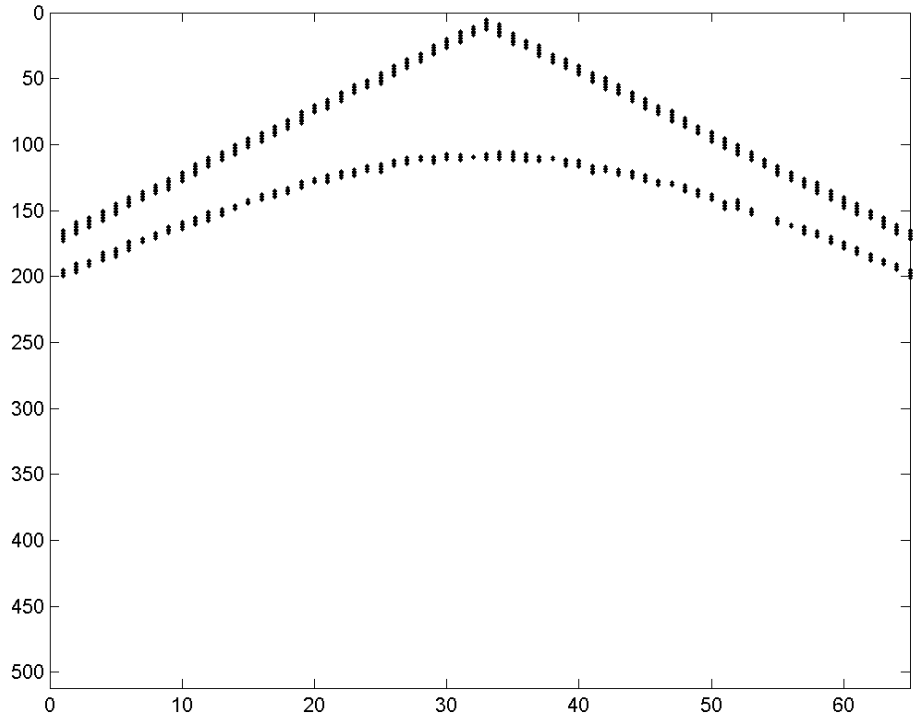

(a)

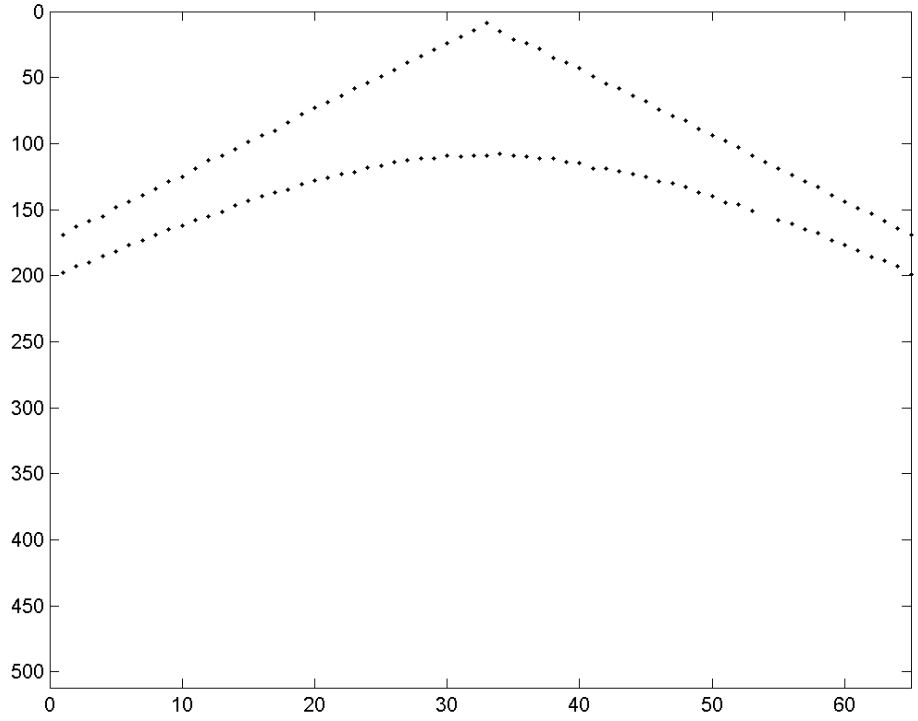

(b)

Fig. 30. (a): Result of thresholding from Fig. 29 with the threshold 0.15. The origin is at the top-left corner. (b): Detected peak from (a).

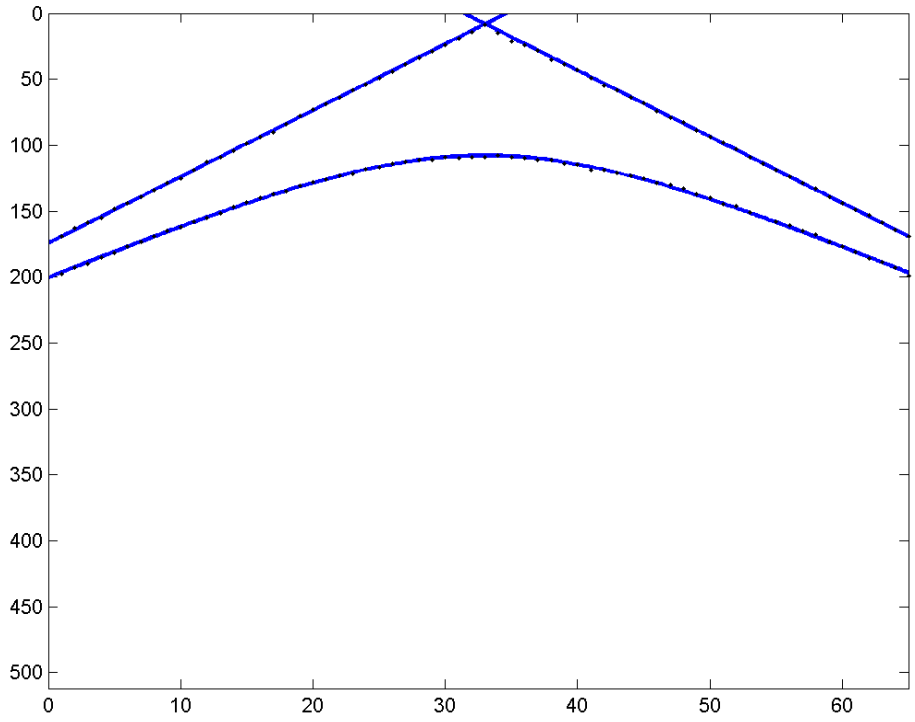

(a)

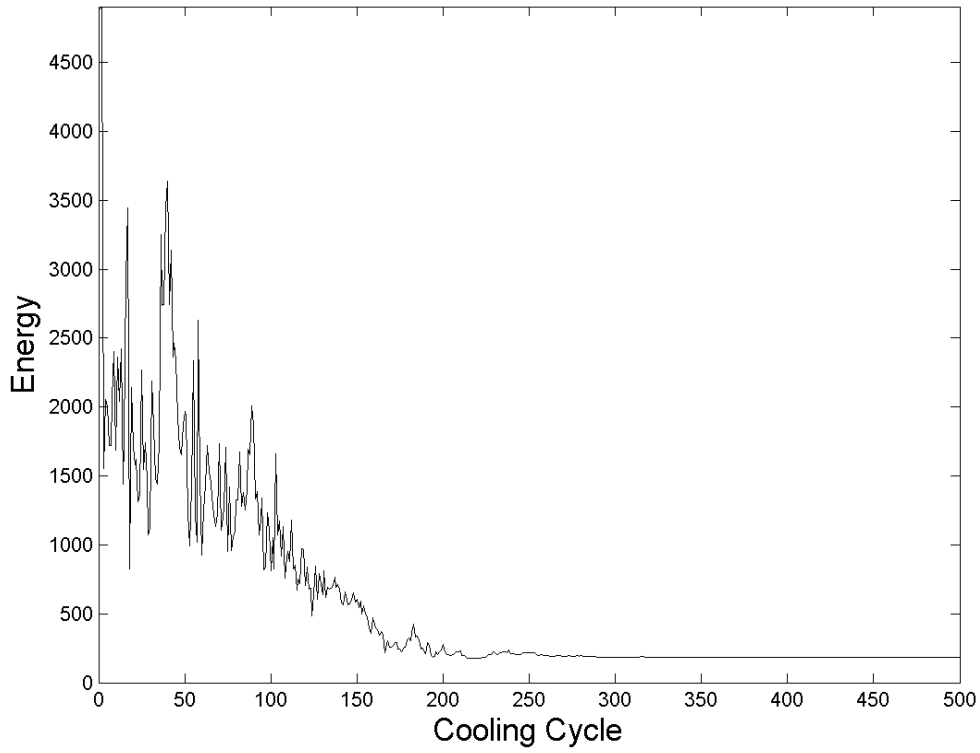

(b)

Fig. 31. Detection of seismic patterns in Fig. 29 − (a): Detection result. (b): Error plot with the cooling cycles.

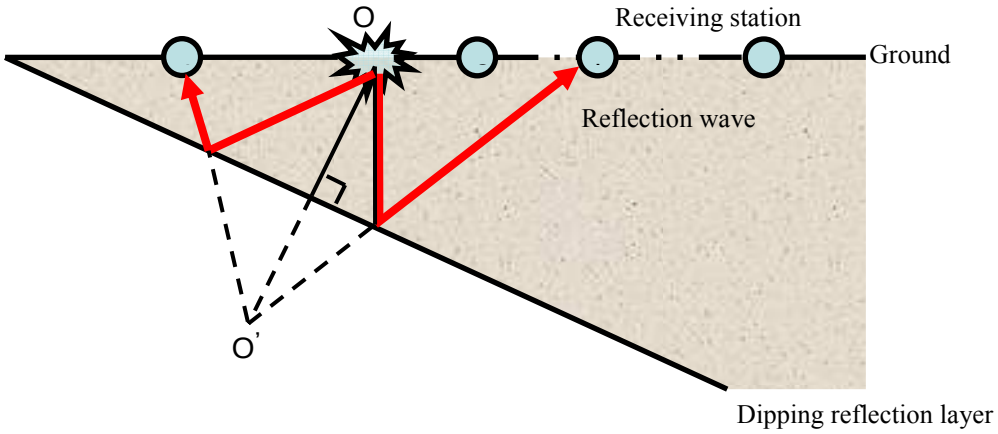

Fig. 32. Illustration of dipping reflection layer.

Fig. 32 illustrates the reflection layer, where the dipping angle is 10° and the depth of the reflection layer is 500m and the velocity of the *p*-wave in the sedimentary rock is about 2,500m/sec [6]. There are 65 receiving stations on both side of explosion with 50m between each others. The sampling interval is 0.004 sec. The impulse response is 25 Hz Ricker wavelet. Reflection coefficient is 0.2 and noise is band-passed noise, 10.2539Hz ~ 59.5703Hz, with uniform distributed over (-0.2, 0.2). Fig. 33 (a) is the simulated one-shot seismogram. Fig. 33 (b) shows the envelope. Fig. 34 (a) is the result of threshold with the threshold 0.15 and Fig. 34 (b) plots the detect peaks.

Points in Fig. 34 (b) are the inputs to the algorithm. The initial parameters $m_{k,x}$ and $m_{k,y}$ are random between 0 and 50, $a_k = -1$, $b_k = 1$, and $f_k = 1$. The cooling function is as (9) with a high enough temperature, $T_{\max} = 600$. There are $Nt = 100$ trials in a temperature. The temperature decreases 500 times. Constants $\alpha_m = 1$, $\alpha_{ab} = 0.5$, and $\alpha_f = 5$. Number of patterns is $K = 2$, and we set $f_1 = 0$ for line patterns of direct wave. Fig. 35 (a) is the detection result of Fig. 34 (b) and Fig. 35 (b) is the corresponding error plot.

Table IV and Table V list the detected parameters for the simulated seismic data.

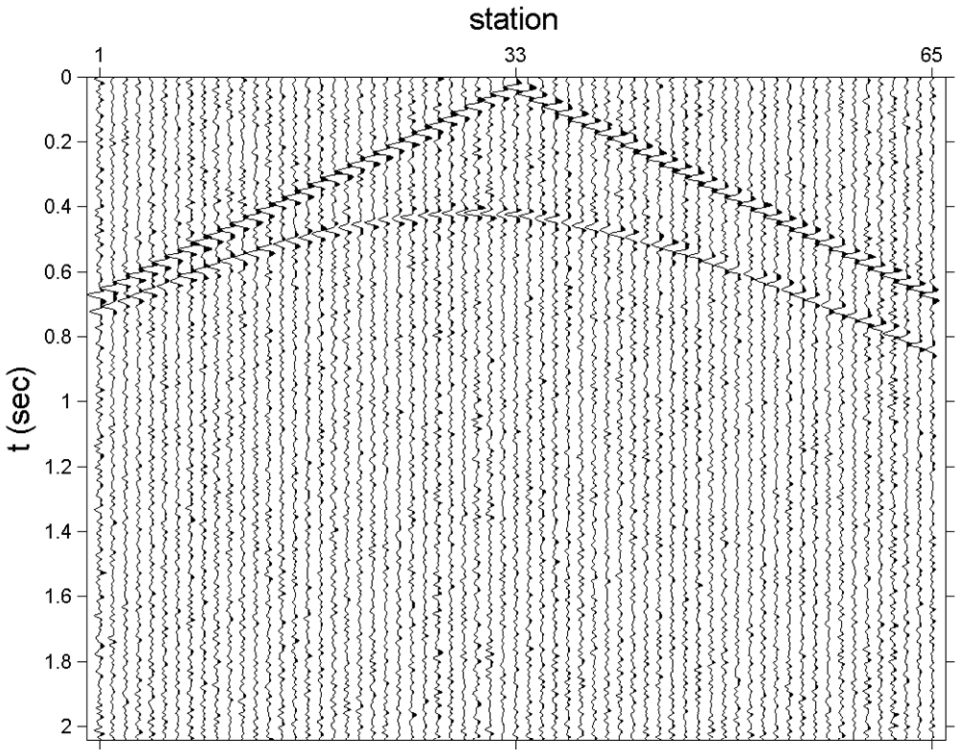

(a)

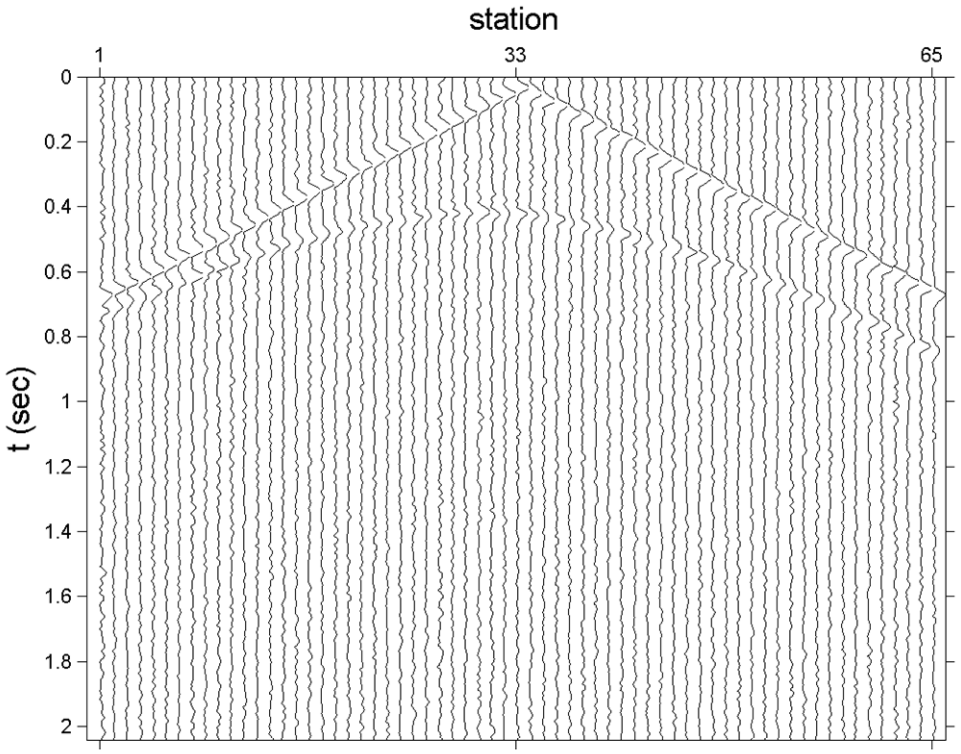

(b)

Fig. 33. Simulated seismic patterns − (a): Simulated one-shot seismogram (dipping reflection layer). (b): After envelope processing.

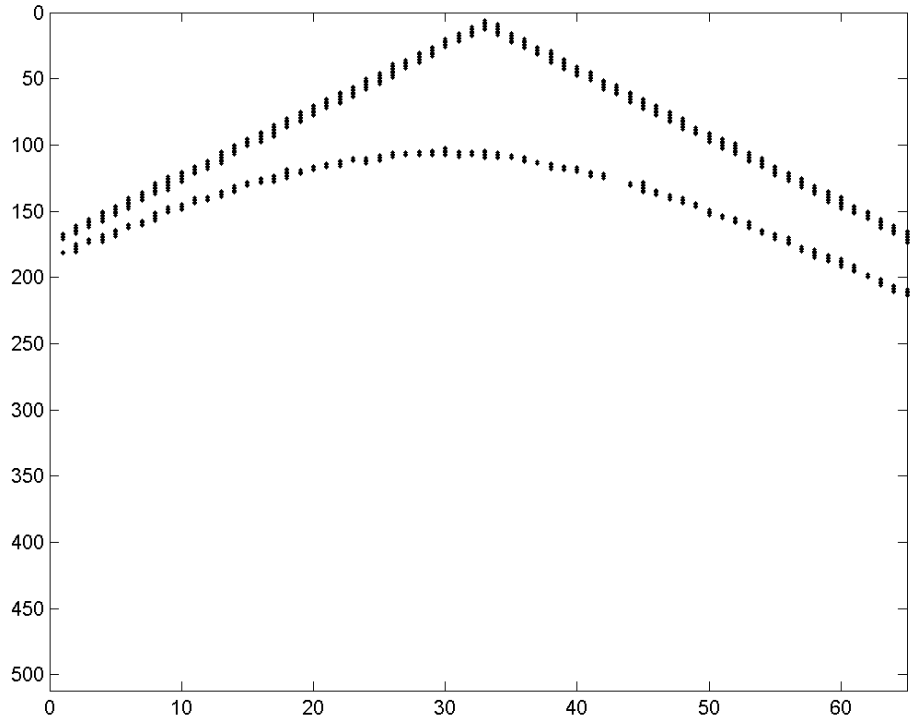

(a)

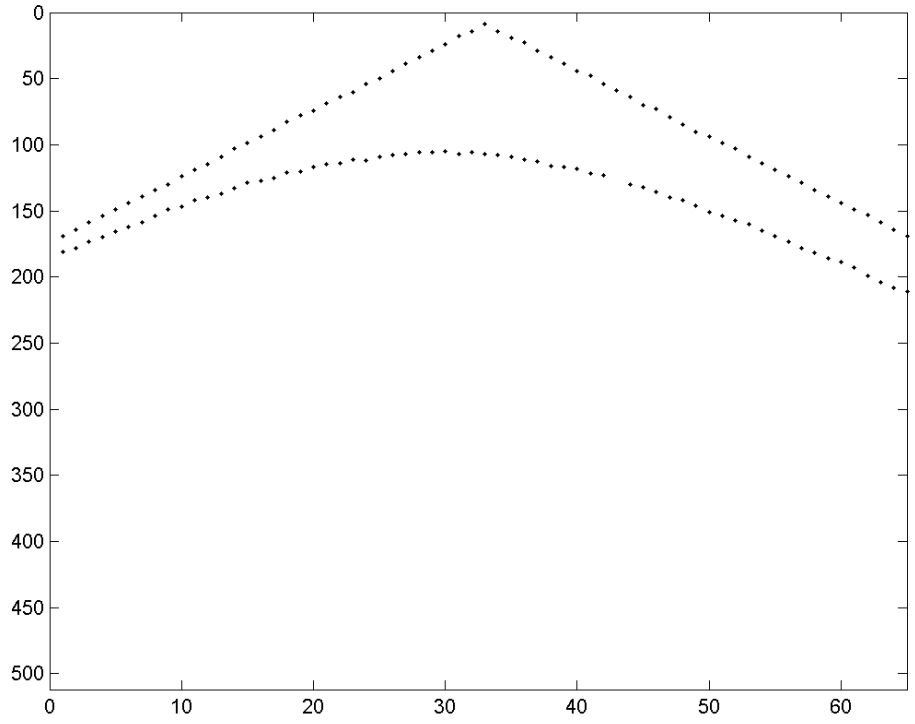

(b)

Fig. 34. (a): result of thresholding from Fig. 33(b) with the threshold 0.15. The original is at the top-left corner. (b): detected peak from (a).

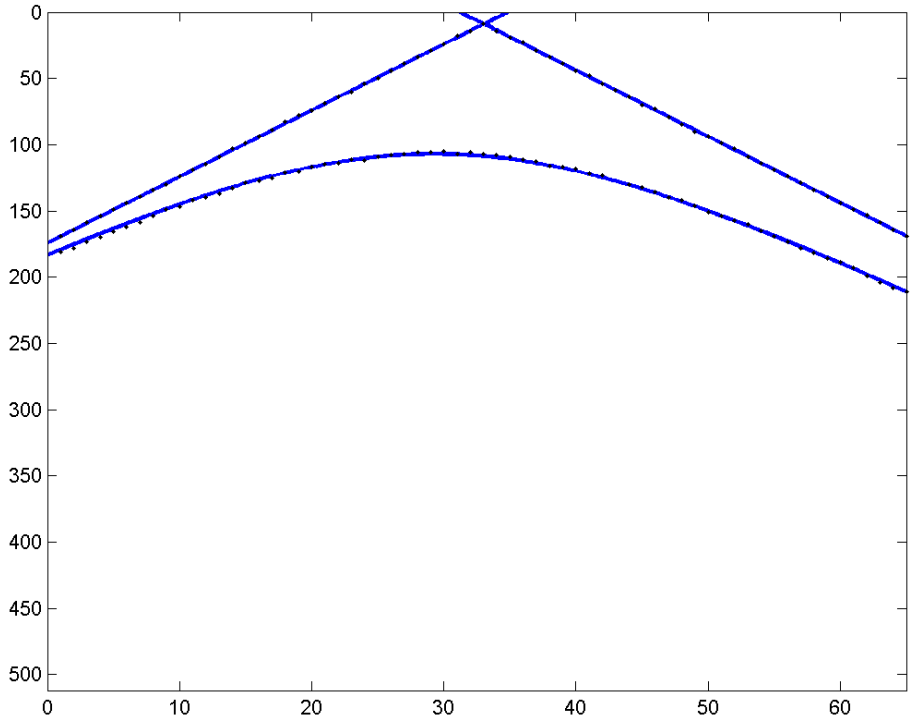

(a)

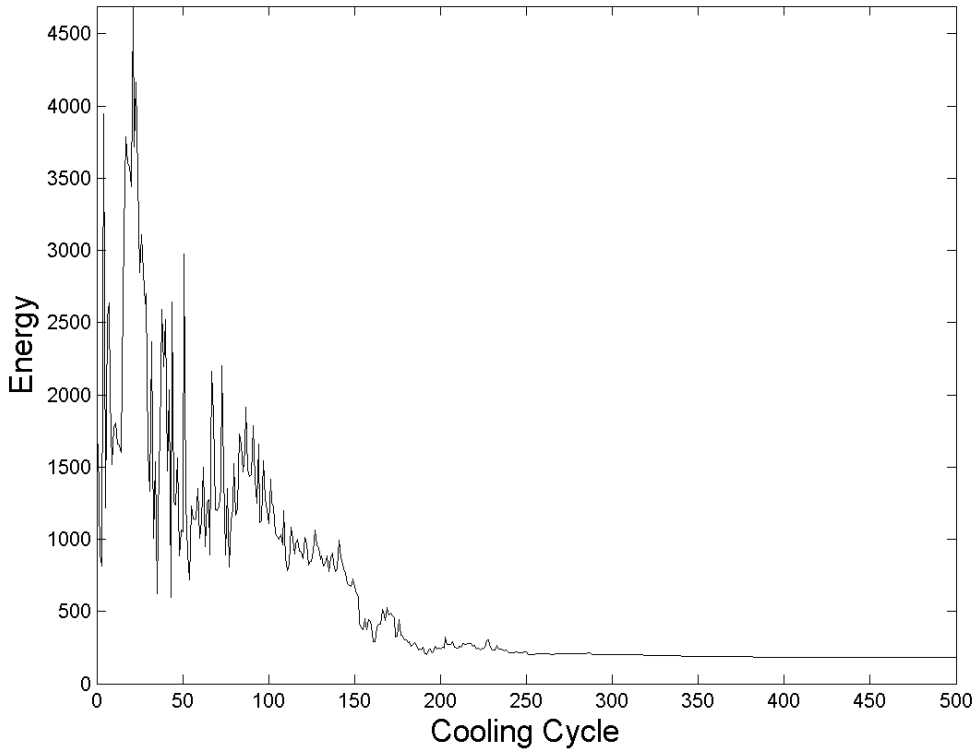

(b)

Fig. 35. Detection of seismic patterns in Fig. 33 − (a): Detection result. (b): Error plot with the cooling cycles.

Table IV

Detected parameters in Fig. 31 (a) in image space 512×65

	m_x	m_y	a	b	f
Direct wave	33.01	8.21	-5.031	0.198	0 (preset)
Reflection wave	32.95	40.09	-4.412	0.226	1040.99

Table V

Detected parameters in Fig. 35(a) in image space 512×65

	m_x	m_y	a	b	f
Direct wave	33.00	8.96	-5.00	0.199	0 (preset)
Reflection wave	29.29	-1.46	-5.115	0.195	2300.17

4.5 *Seismic Applications on Real Seismic Data*

The system is also applied to detect direct wave and reflection wave in real seismic data. We obtain data from Seismic Unix System developed by Colorado School of Mine [5].

The real data with the size 3100×48 showed in Fig. 36 (a) is from Canadian Artic, which has 48 traces and 3100 samples per trace with sampling interval 0.002 seconds. The horizontal axis is the trace number and the vertical axis is time t.

After envelope and threshold preprocessing [7], Fig. 36 (b) shows the result of envelope and Fig. 37 (a) shows the result of thresholding with the threshold 0.15. The result of peak detection is in Fig. 37 (b). We only choose points with $y < 700$ which includes points from direct wave, first reflection wave and second reflection wave as in Fig. 38 (a) where there are 88 points. Detected curves are plotted in Fig. 38 (b) with $K = 3$ and we preset $f_1 = 0$. Here, the initial parameters $m_{k,x}$ and $m_{k,y}$ are random number between 0 and 50, $a_k = -1$, $b_k = 1$, and $f_k = 0$. The cooling function is as (9) with a high enough temperature, $T_{\max} = 1{,}000$. There are $Nt = 100$ trials in a temperature, and the temperature decreases 500 times. Constants settings: $\alpha_m = 1$, $\alpha_{ab} = 0.5$, and $\alpha_f = 10$.

Since the second reflection wave is not a hyperbola in theory [3], we remove the points from the second-layer reflection wave. That is, we remove the points nearest to the bottom pattern in Fig. 38 (b). Remaining 65 points are plotted in Fig. 39 (a). We redo the experiment, and this time $K = 2$. Fig. 39 (b) shows the result. The detected parameters in Fig. 38 (b) and Fig. 39 (b) are listed in Table VI and Table VII.

Table VI

Detected parameters in Fig. 38 (b) with fixed $f_1 = 0$ in image space 3100×48

	m_x	m_y	a	b	f
Direct wave	24.48	8.59	-25.69	0.038	0 (preset)
Reflection wave	24.83	28.83	-22.91	0.044	2,441.7
Second Reflection wave	24.74	49.59	-23.10	0.043	8,942.7

Table VII

Detected parameters in Fig. 39 (b) with fixed $f_1 = 0$ in image space 3100×48

	m_x	m_y	a	b	f
Direct wave	24.53	11.20	-25.59	0.039	0 (preset)
Reflection wave	24.62	-2.81	-24.13	0.041	2,978.05

As mentioned in [3]-[5], two lines of direct wave is a pair of asymptotes of the hyperbola and a pair of asymptotes is a hyperbola with size zero. From the detected parameters in Table VIII, we obtain the equation of the direct wave

$$\begin{aligned} &-25.59(x-24.53)^2 + 0.039(y-11.20)^2 = 0 \\ &\Rightarrow 25.59(x-24.53)^2 = 0.039(y-11.20) \end{aligned} \tag{20}$$

Rearrange (20) and take square root on both sides, the equations of two lines in image space are

$$\begin{aligned} 5.0587x - 0.1975y &= 121.8779 \\ 5.0587x + 0.1975y &= 126.3019 \end{aligned} \tag{21}$$

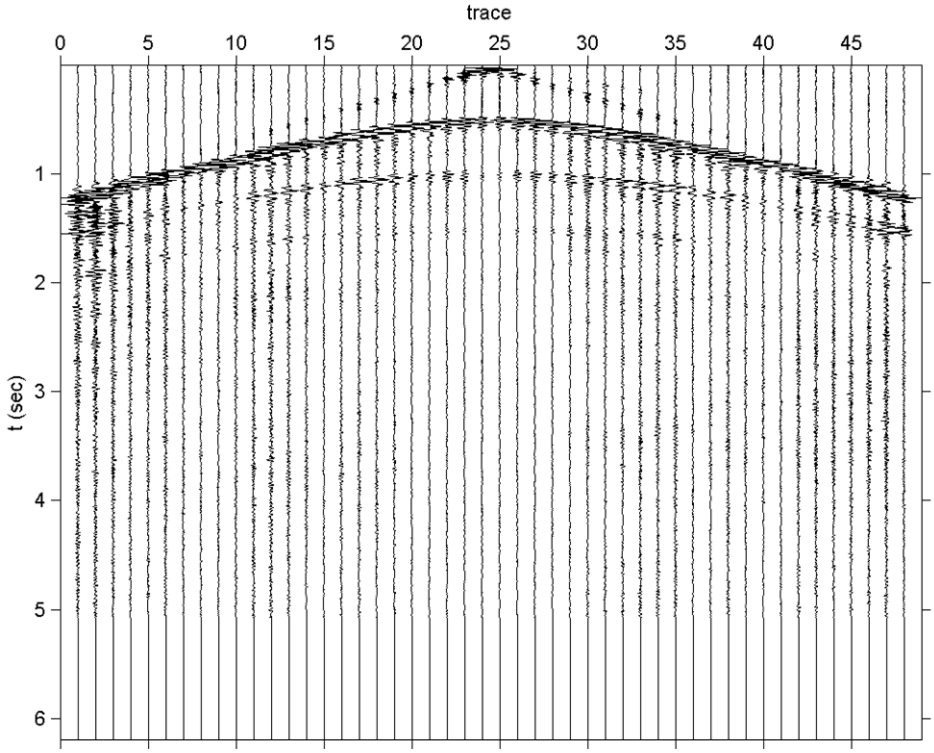

(a)

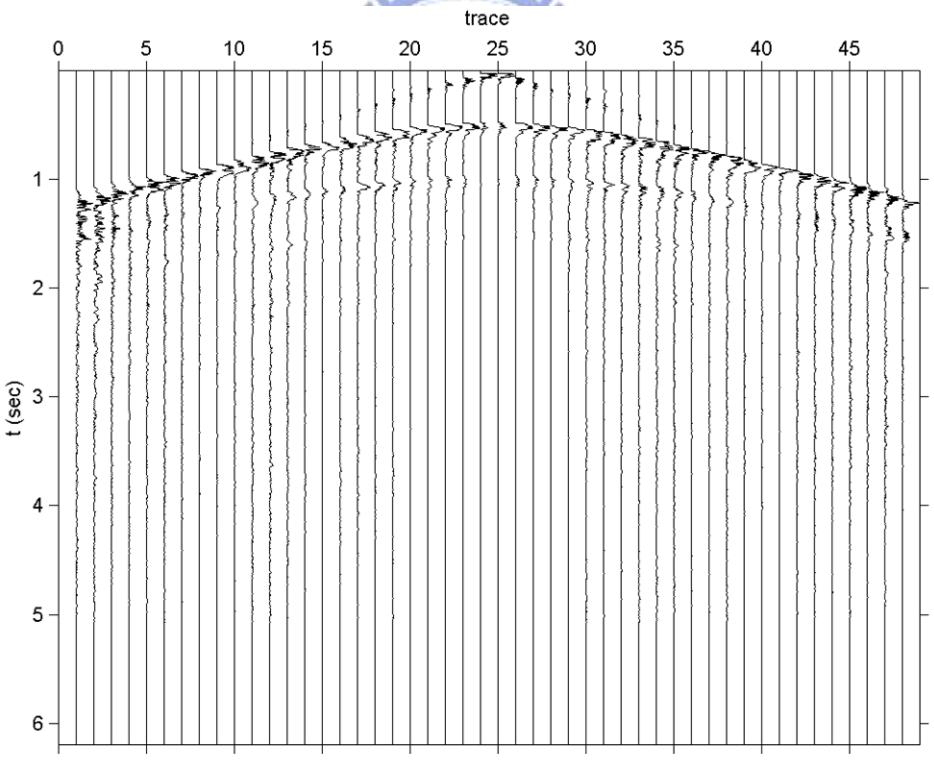

(b)

Fig. 36. Experiment on real data -- (a): Real seismic data from Canadian Artic. (b): Plot of envelope.

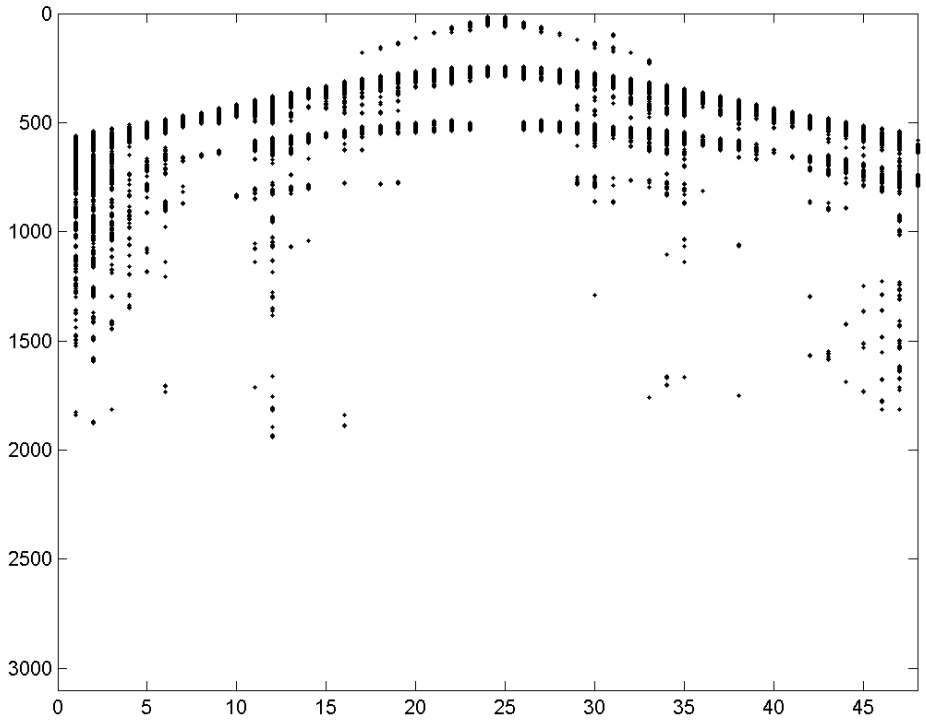

(a)

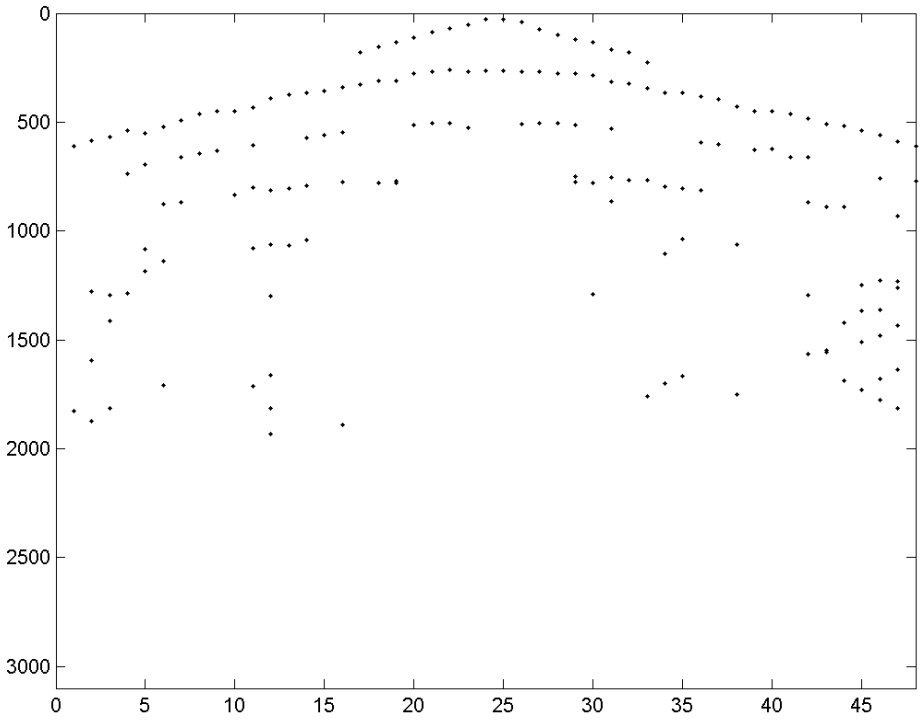

(b)

Fig. 37. Experiment on real data -- (a): Threshold 0.15. (b): Detect peak.

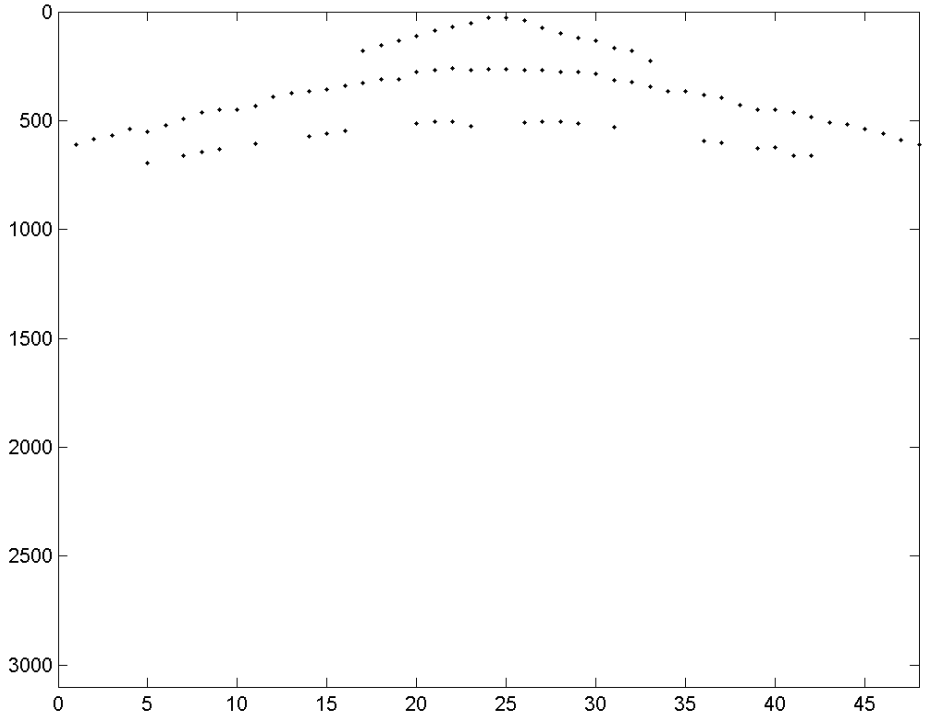

(a)

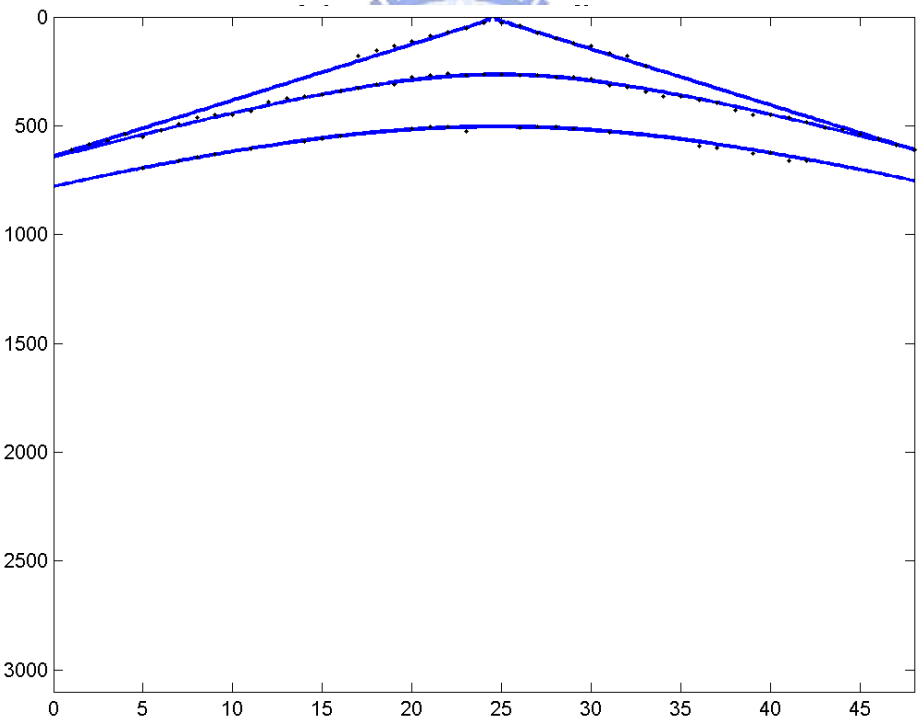

(b)

Fig. 38. Experiment on real data -- (a): Choose peak with $y < 700$. (b): Detection result of (a).

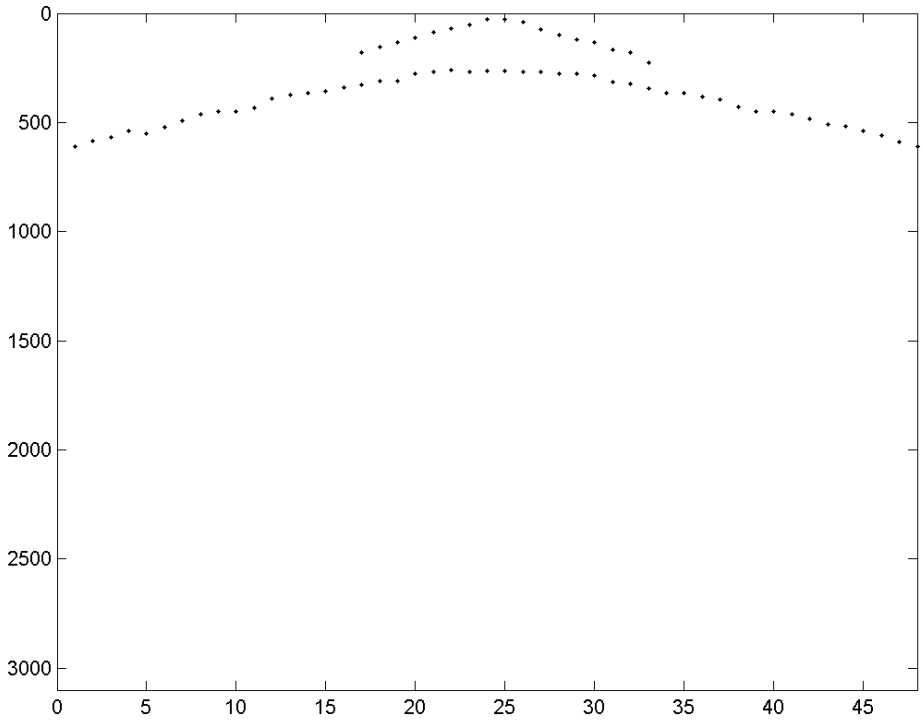

(a)

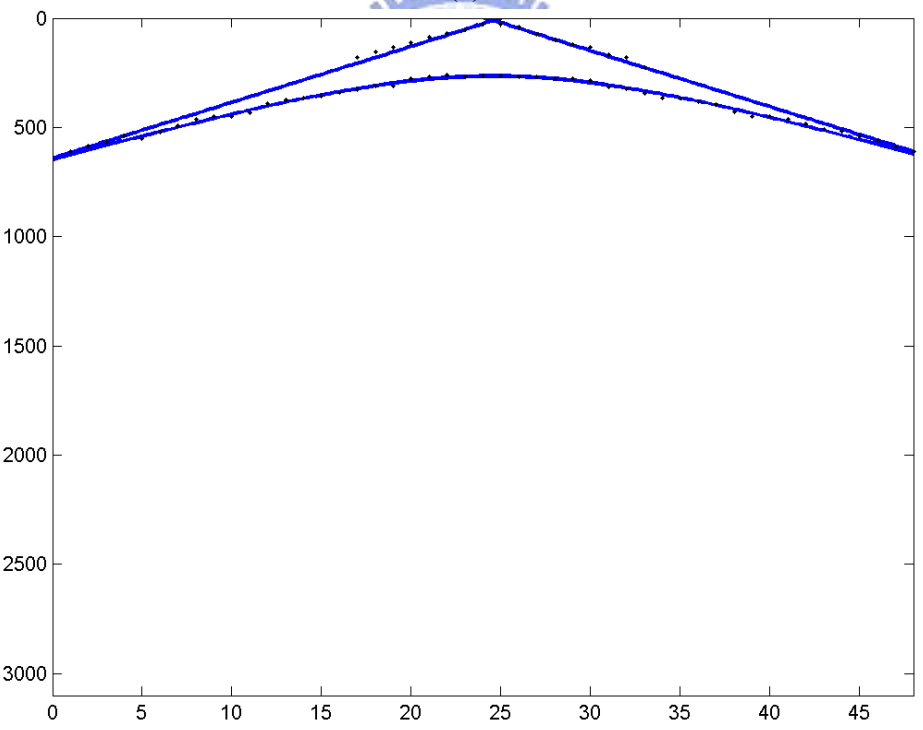

(b)

Fig. 39. Experiment on real data -- (a): Remove points nearest to the bottom pattern. (b): Detection result.

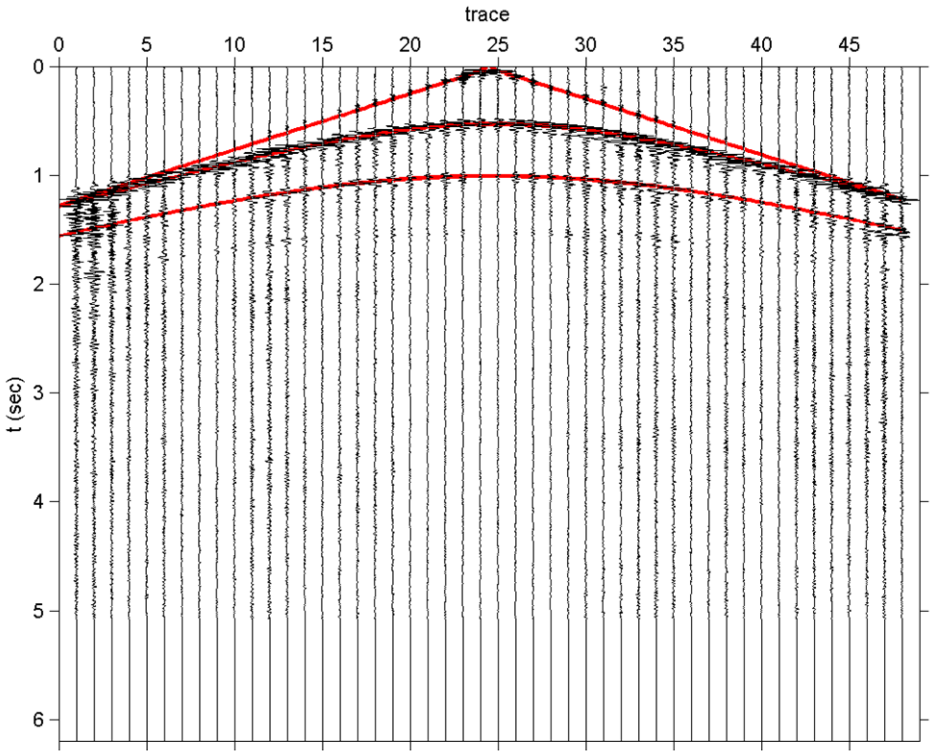

(a)

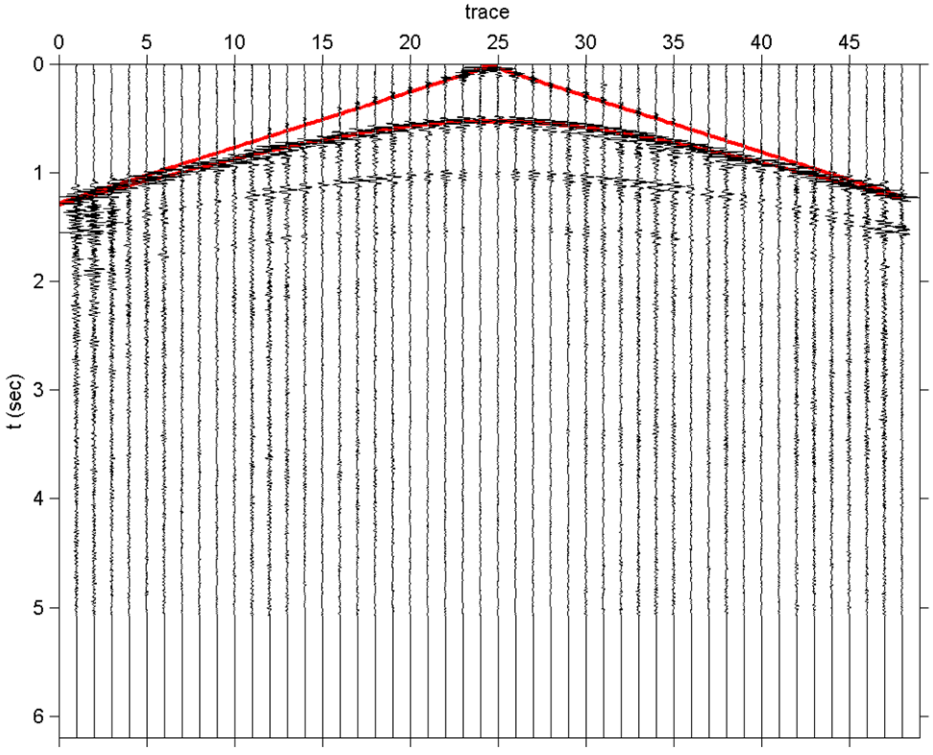

(b)

Fig. 40. Plot detected curve on the original data -- (a): Detection result from Fig. 38 (b). (b): Detection result from Fig. 39 (b).

The other real data is Gulf of Cadiz's seismic data. There are 48 traces and 2050 samples in a trace with sampling interval 0.004 seconds. Fig. 41 (a) shows the real data. The horizontal axis is the trace number and the vertical axis is time t.

After envelope and threshold preprocessing [7], Fig. 41 (b) shows the envelope and Fig. 42 shows the thresholding result with threshold 0.5. The detected peak in Fig. 42 are plotted in Fig. 43 (a) where there are 66 points and the size of image is 2050×48, where the horizontal axis is x and the vertical axis is y. The initial parameters $m_{k,x}$ and $m_{k,y}$ are random number between 0 and 50, $a_k = -1$, $b_k = 1$, and $f_k = 0$. The cooling function is as (9) with a high enough temperature, $T_{\max} = 1{,}000$. There are $Nt = 100$ trials in a temperature. The temperature decreases 500 times. Constants settings: $\alpha_m = 1$, $\alpha_{ab} = 0.5$, and $\alpha_f = 10$. Number of patterns is $K = 2$. The detection result is in Fig. 43 (b).

Since the points nearest to the pattern around $y = 800$ are from second-layer reflection wave. In theory, the second-layer reflection wave is not a hyperbola [3]. We remove those points and remaining 48 points are plotted in Fig. 44 (a). Fig. 44 (b) shows the detection result and Fig. 45 plots the detected curve in the original data. Table VIII and Table IX list the detected parameters in image space in Fig. 43 (b) and Fig. 44 (b).

Table VIII

Detected parameters in Fig. 43 (b) in image space 2050×48

	m_x	m_y	a	b	f
Reflection wave	44.57	187.84	-6.93	0.144	2,116.8
Second-layer reflection wave	21.64	56.27	-25.13	0.040	12,537.7

Table IX

Detected parameters in Fig. 44 (b) in image space 2050×48

	m_x	m_y	a	b	f
Reflection wave	45.58	174.02	-7.00	0.143	2,519.30

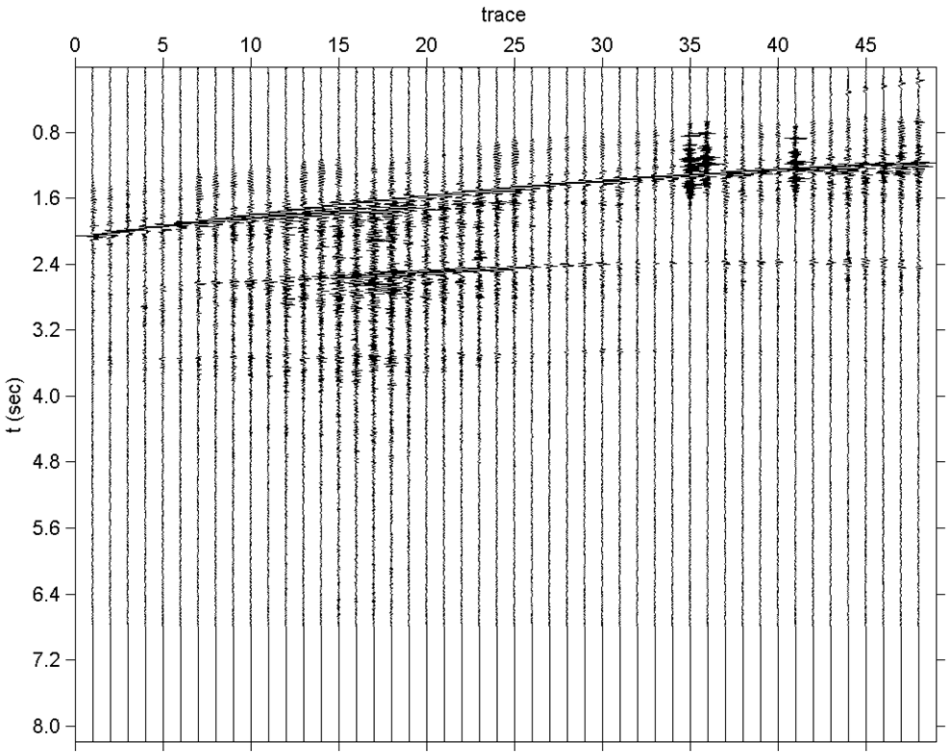

(a)

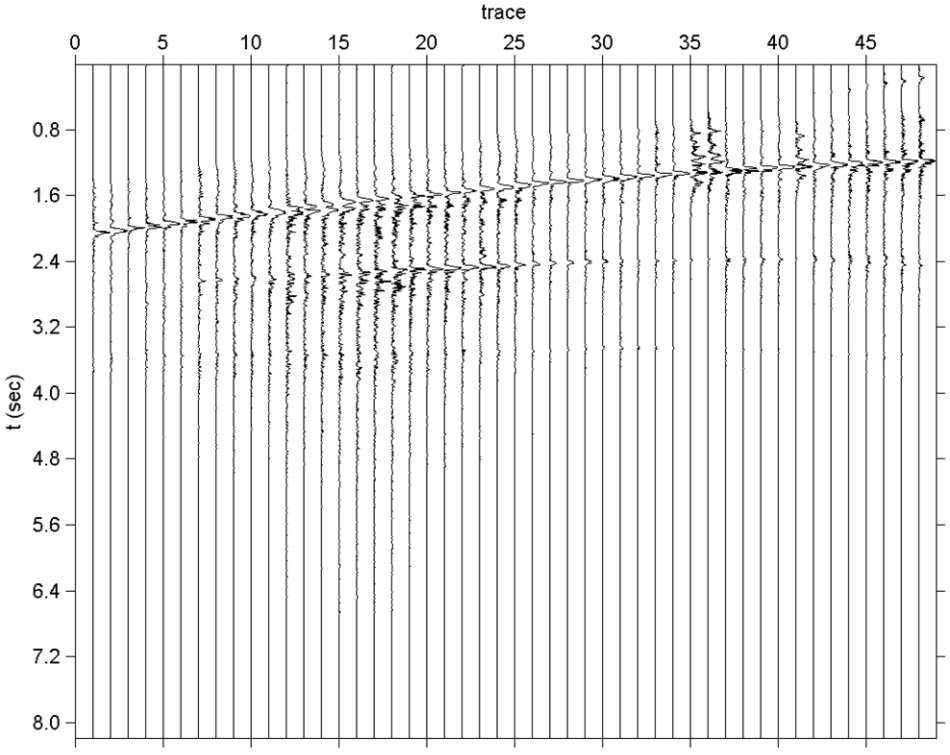

(b)

Fig. 41. Experiment on real data -- (a): Real seismic data from Gulf of Cadiz. (b): Plot of envelope.

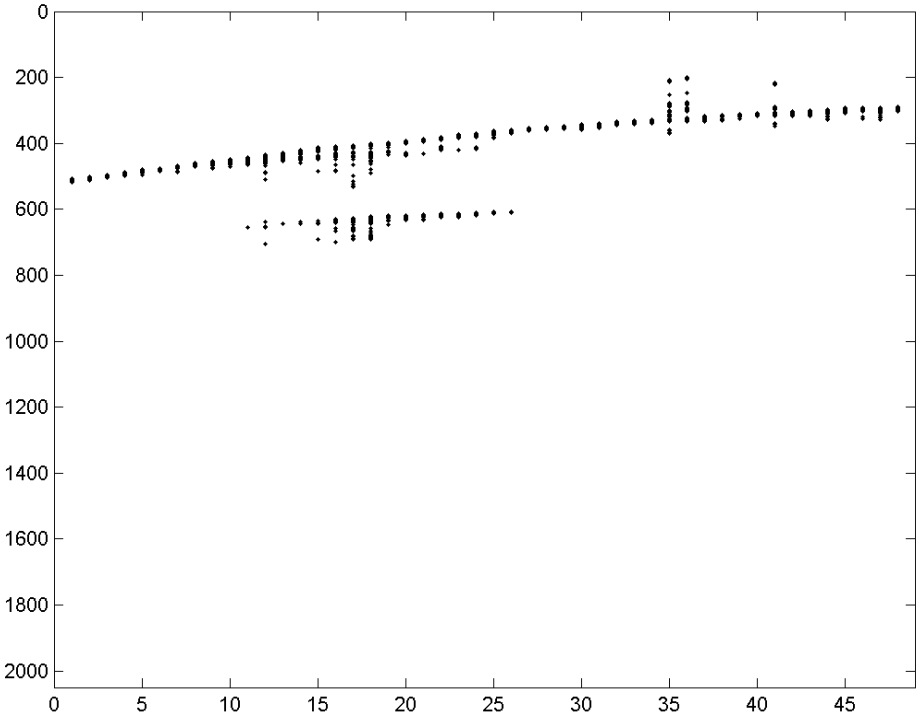

(a)

Fig. 42. Experiment on real data – Thresholding result of the envelope in Fig. 41 (b) with threshold 0.5.

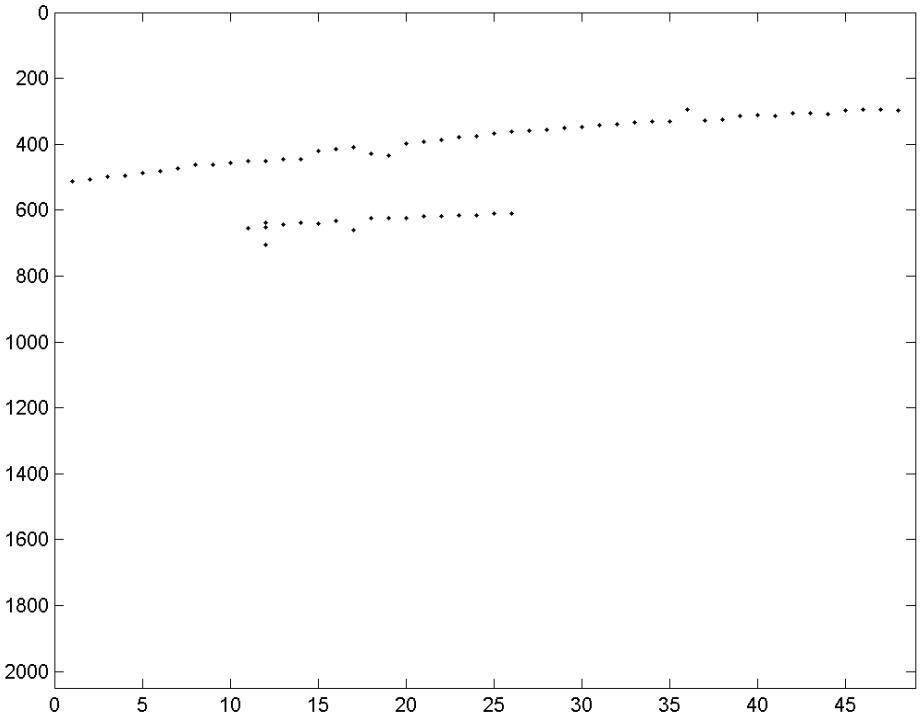

(a)

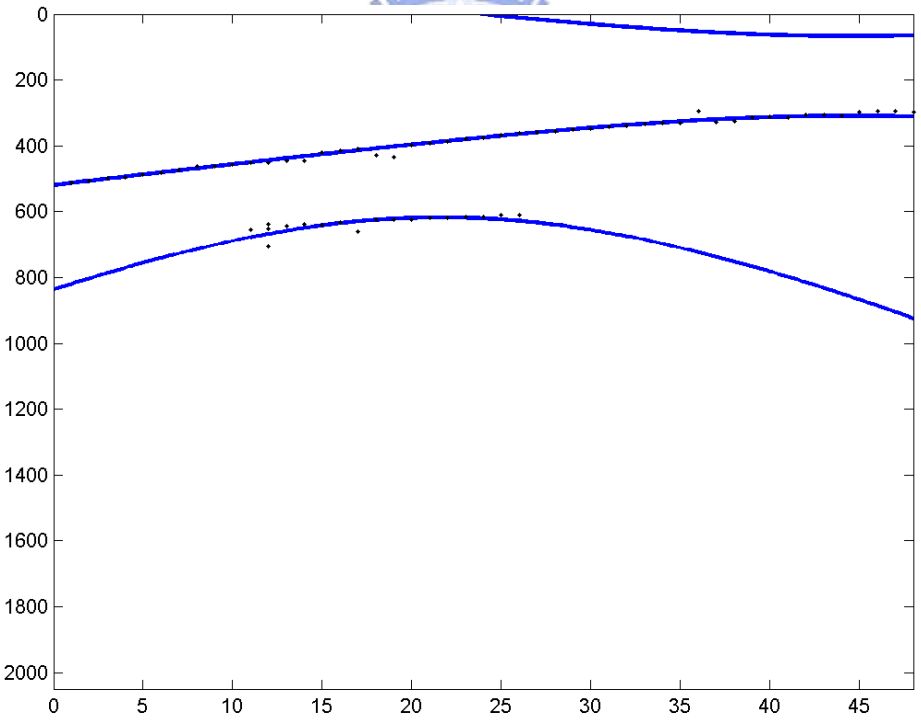

(b)

Fig. 43. Experiment on real data -- (a): Detected peak from Fig. 42. (b): Detection result of (a), $K = 2$.

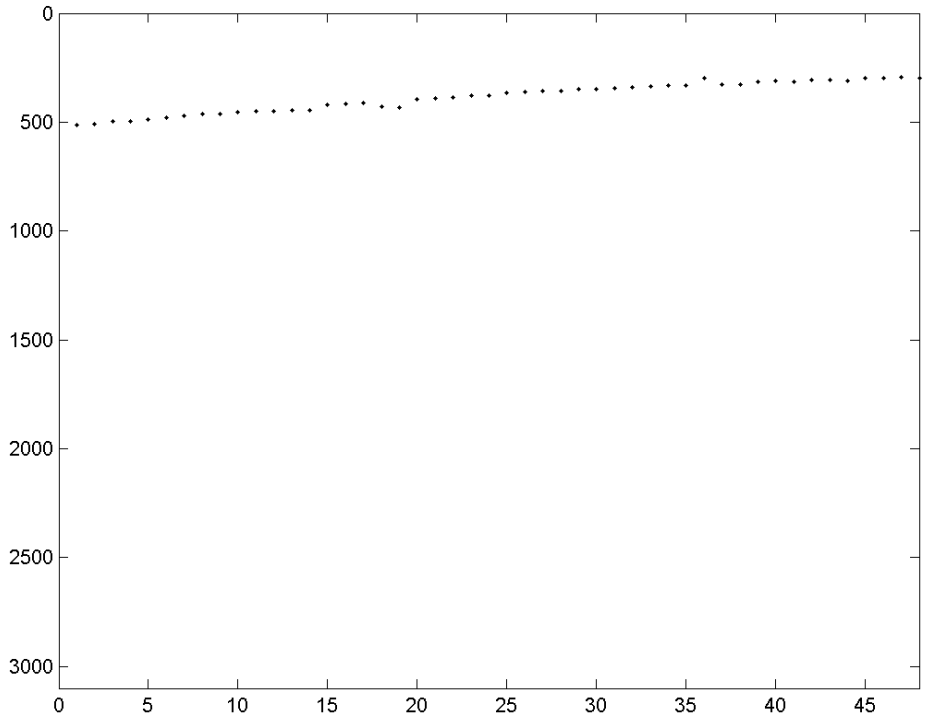

(a)

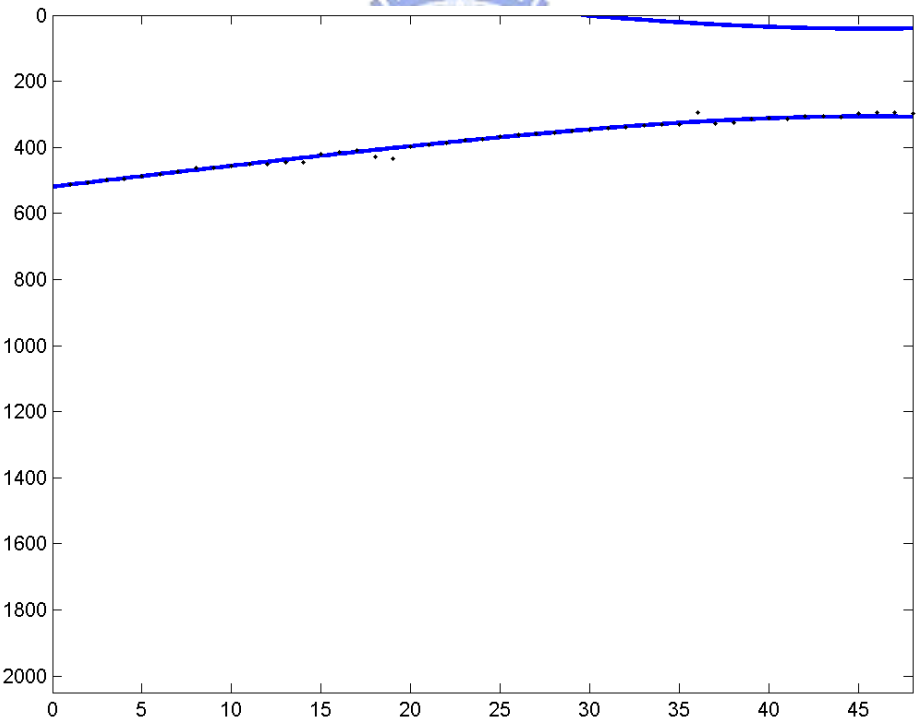

(b)

Fig. 44. Experiment on real data -- (a): Remove points nearest to the pattern around y = 800 in Fig. 43 (b). (b): Detection result of (a), K = 1.

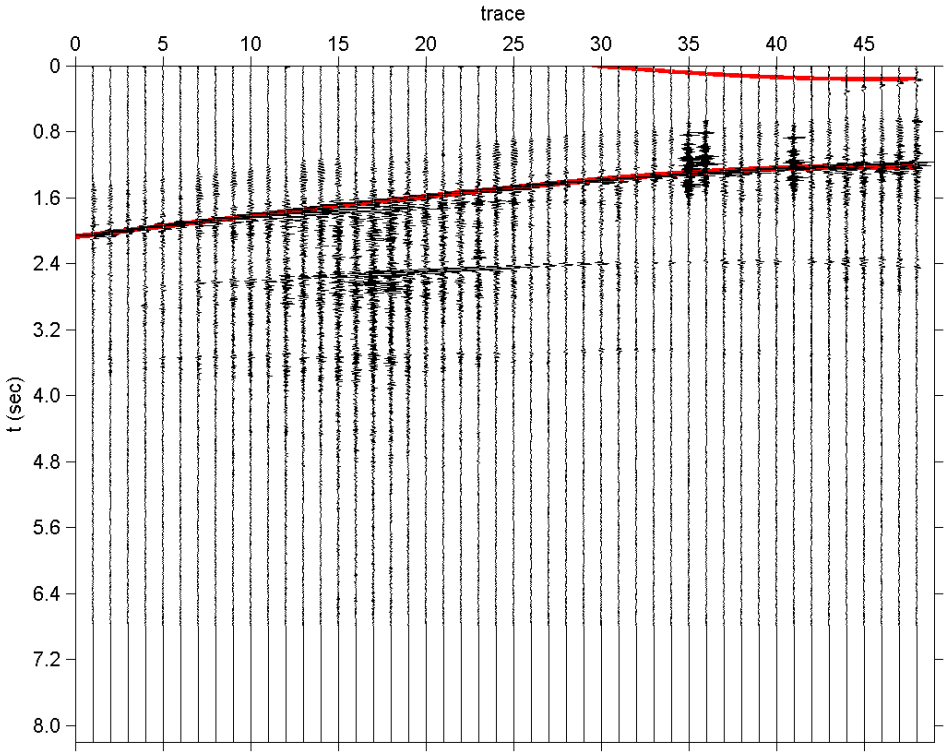

Fig. 45. Plot the detected curve in Fig. 44 (b) on the original data.

Chapter 5

Conclusions and Discussions

5.1 *Conclusions*

This paper is about a proposed system, which adopted the simulated annealing algorithm to detect patterns such as lines, circles, ellipses, and hyperbolas by finding their parameters in an unsupervised manner and global minimum fitting error related to points in an image. The iterative adjustment requires less memory space. Also, we define the distance from a point to a pattern and this makes the computation feasible, especially for hyperbola. Using four steps to adjust parameters from center, shape, angle to the size of the pattern can get fast convergence. Based on the average minimum distance from points to patterns, we have proposed a method to determine the number of patterns automatically. Experimental results on the detection of line, circle, ellipse, and hyperbola in images are successful. The detection results of line pattern of direct wave and hyperbolic pattern of reflection wave in one-shot seismogram are good, and can improve seismic interpretations and further seismic data processing.

5.2 *Discussions*

Parameter settings. In the cooling schedule, the value of T_{max}, and Nt, are set prior.

For a trial which includes a change of center, a change of b and a, a change of θ, and a change of f for every pattern, there are three possible results to accept or reject the change determined by Metropolis criterion:

1. The new parameter has smaller error and it is accepted.
2. The new parameter has larger error and it is still accepted.
3. The new parameter has larger error and it is rejected.

The determination of T_{max}, we considered the accept ratio of the larger-error trials. If the T_{max} is not high enough, the trial with larger error will almost reject, that is, it always accept trial with smaller error, so it is possible to reach local minimum. Fig. 46 shows this situation, where T_{max} = 1,500 iterations, initial center (0,0), a = 1, b = 1, θ

= 0, and f = 1. Fig. 47 shows the result when T_{max} = 10. In Fig. 47 (b), the accept ratio of canter, angle, and size has increased and shows the good result for this simple example. Fig. 48 show the result when T_{max} = 100,000. After 500 iterations, T = 4.1, but this temperature is not low enough and the high accept ratio of larger-error parameters results in the instability. To solve this problem, we can increase the number of iterations to 1,000 and show the result in Fig. 49. This still shows good result, but it takes more time. In conclusions, for temperature T_{max}, we have to choose a high enough temperature that gives a high accept ratio of larger-error parameters. Besides, we need many enough iterations to cool the temperature to ensure stability.

Also we find the setting of T_{max} is proportional to the scale of input points. In Fig. 47, T_{max} = 10 provides good result. In Fig. 50, we enlarge the scale of data by two. Fig. 50 (a) with T_{max} = 10 cannot give good result, but Fig. 50 (a) with T_{max} = 100 can give good result. In our simulation experiments, we choose T_{max} = 500 and 500 iterations to ensure high enough initial temperature and lower final temperature $T \approx$ 0.02.

As for Nt, if trials are not many enough, we cannot get good result. Larger Nt takes more time but gives more chances. So we can have as many trials as possible if the computational power is strong enough. Fig. 51 shows too few trials cannot provide good result and for this simple example we need only Nt = 10 to obtain a good result.

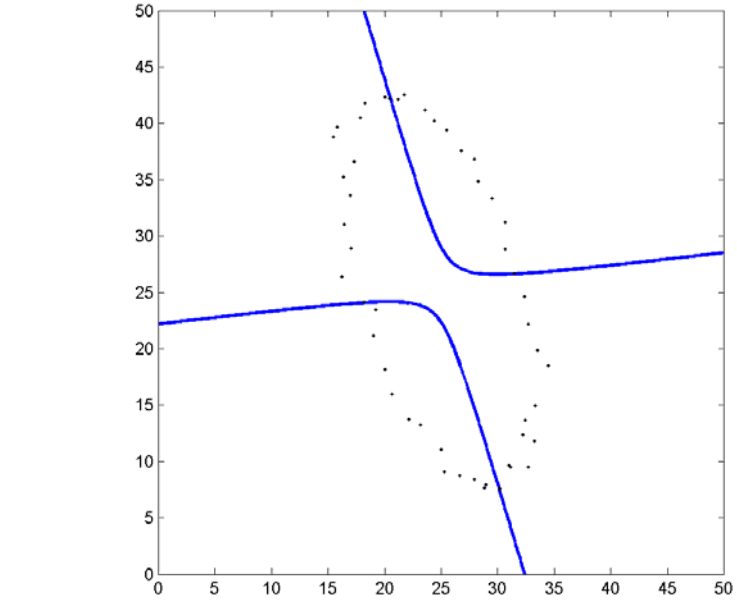

(a)

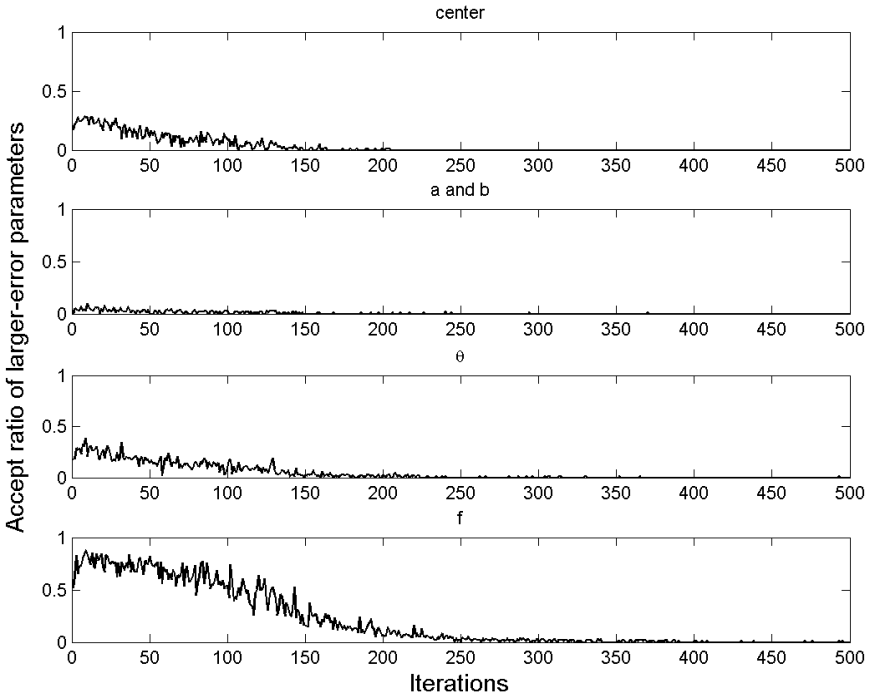

(b)

Fig. 46. Illustration of low initial temperature T_{max}: (a) Detection result of T_{max} = 1. (b) Accept ratio of larger-error parameters.

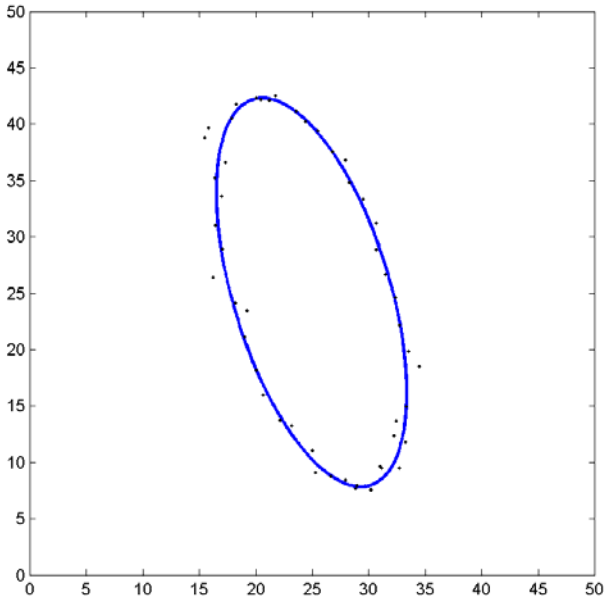

(a)

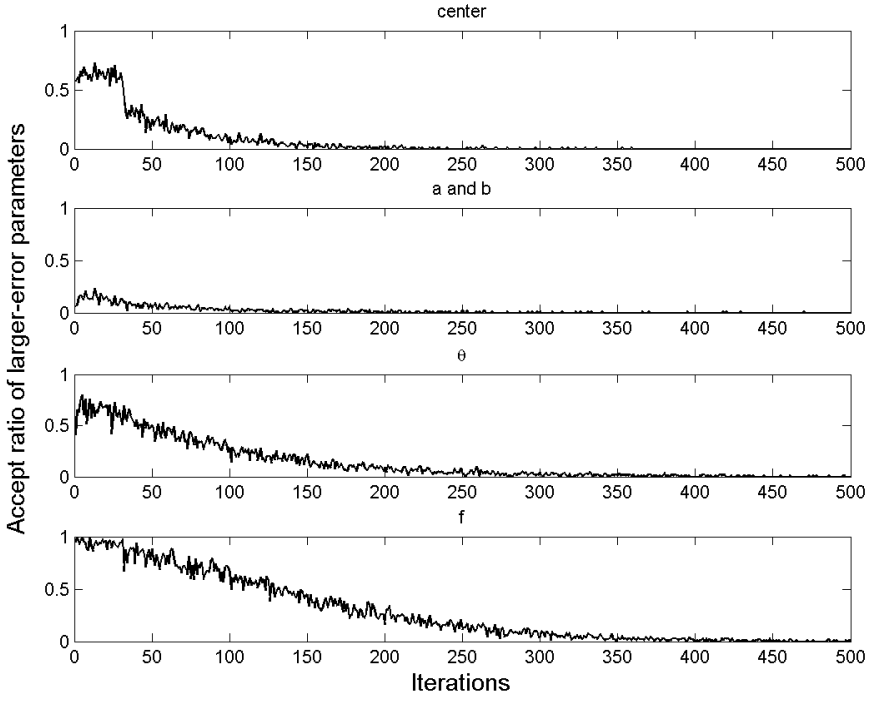

(b)

Fig. 47. Illustration of low initial temperature T_{max}: (a) Detection result of T_{max} = 10. (b) Accept ratio of larger-error parameters.

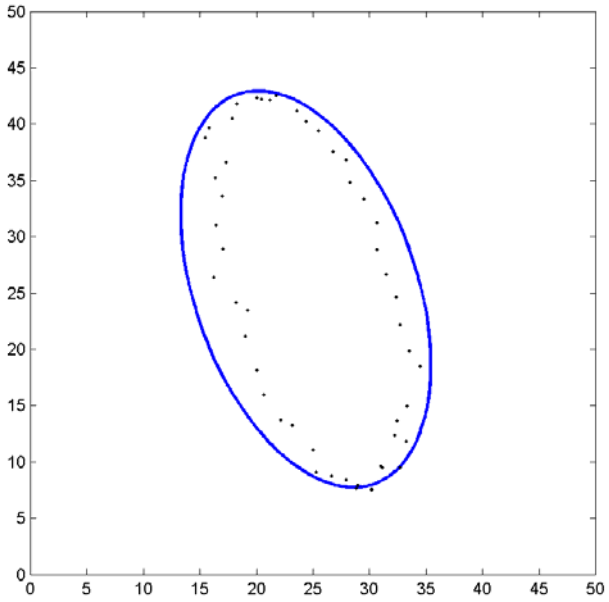

(a)

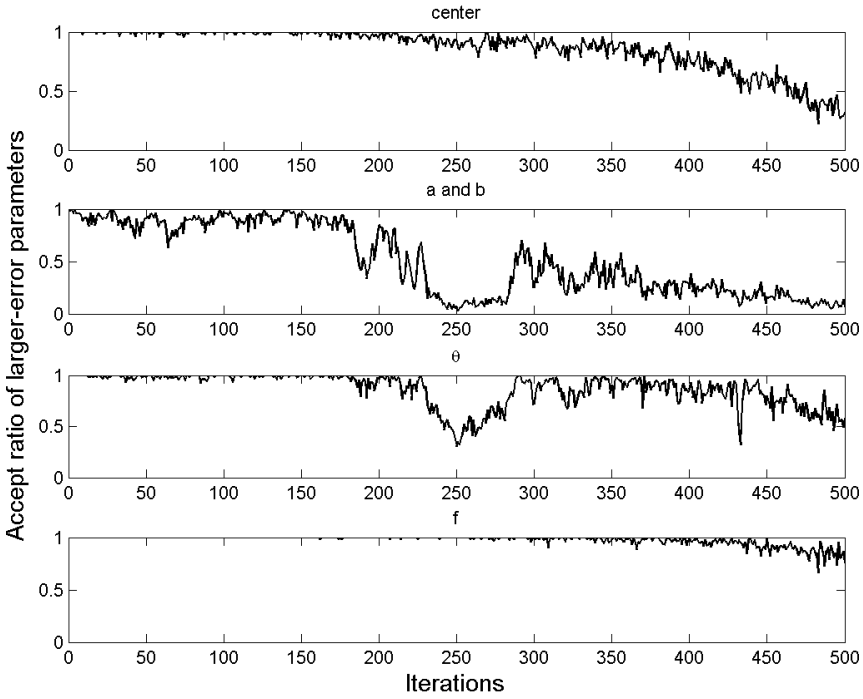

(b)

Fig. 48. Illustration of high initial temperature T_{max}: (a) Detection result of T_{max} = 100,000. (b) Accept ratio of larger-error parameters.

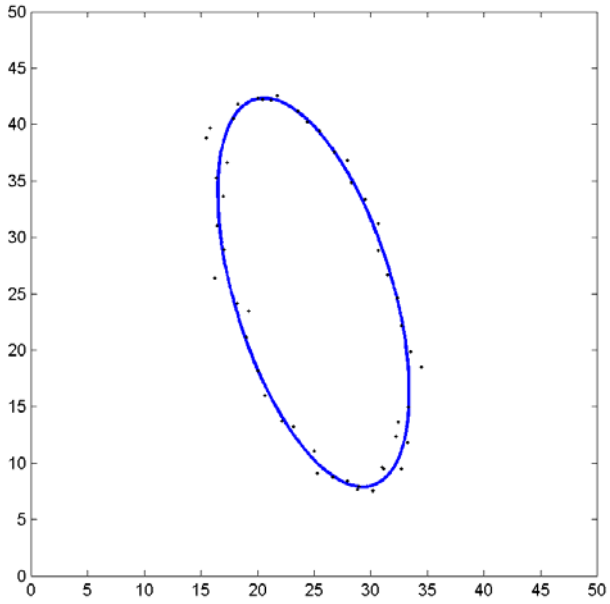

(a)

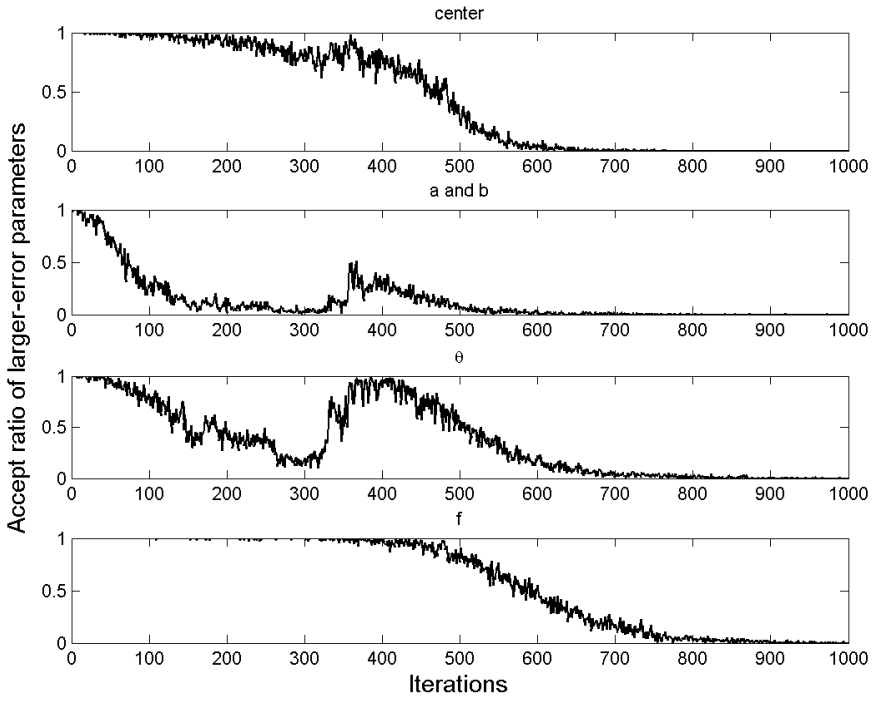

(b)

Fig. 49. Illustration of high initial temperature T_{max} with more iterations: (a) Detection result of T_{max} = 100,000. (b) Accept ratio of larger-error parameters.

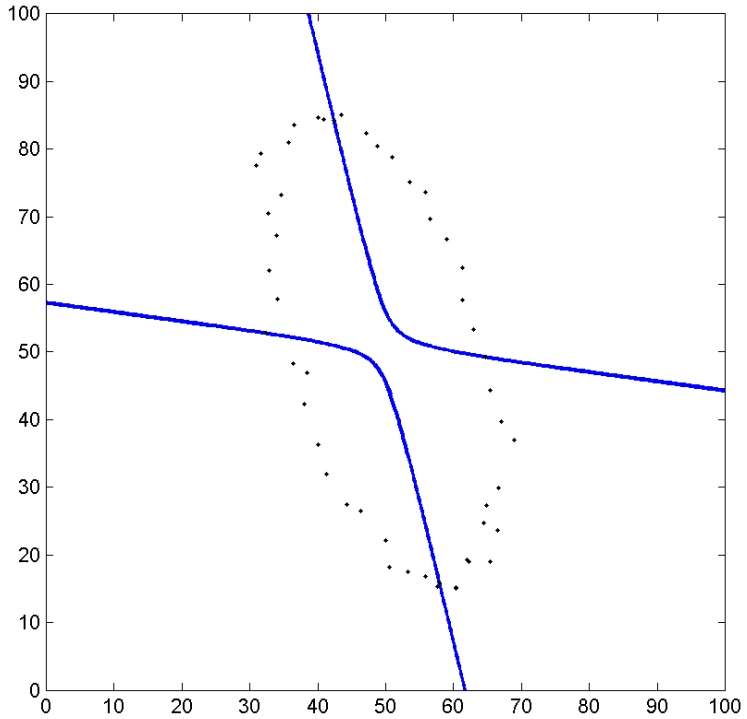

(a)

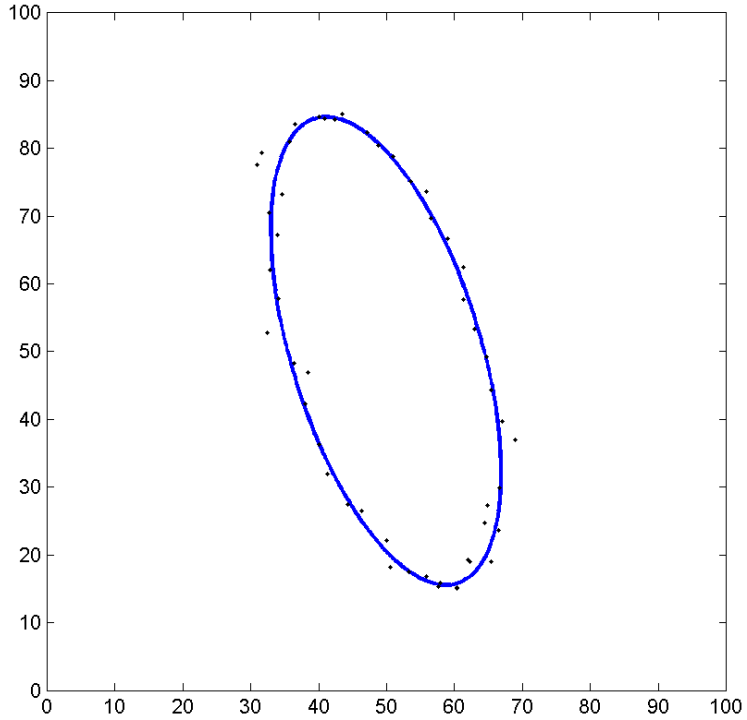

(b)

Fig. 50. Enlarge the scale of points by two: (a) Detection result of $T_{\max} = 10$. (b) Detection result of $T_{\max} = 100$.

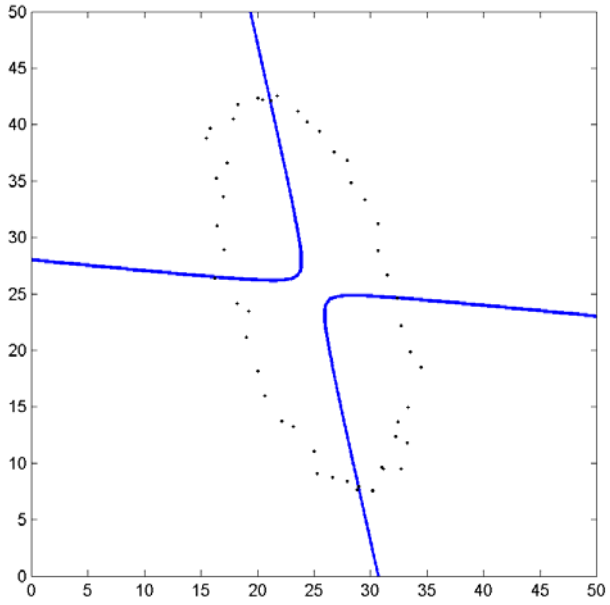

(a)

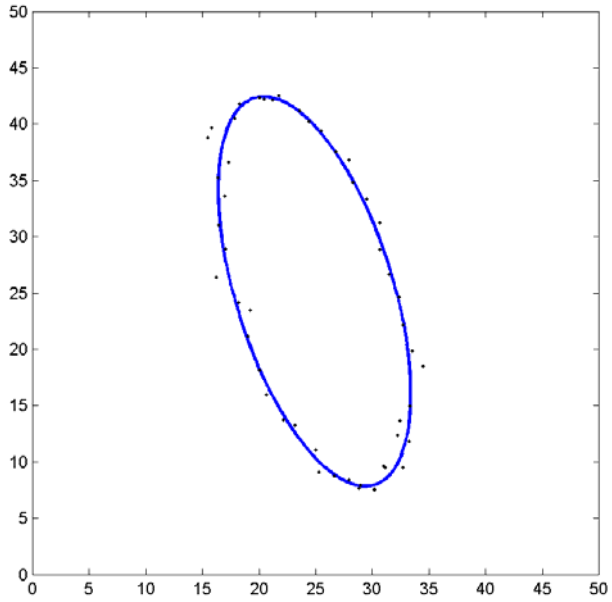

(b)

Fig. 51. Relationship between Nt and detection result $T_{\max} = 500$: (a) Detection result of $Nt = 1$. (b) Detection result of $Nt = 10$.

Time consumption. As for the time consumption, Table III shows that the CPU time is proportional to the number of patterns or the number of parameters. The larger number of parameters, the algorithm takes more time to obtain the solution.

Memory requirement. For traditional HT, it needs an accumulation matrix. The size of accumulation matrix grows as the number of parameters increases. Besides,

the higher precision, the larger accumulator matrix is needed. On the other hand, SA algorithm for parameter detection needs only memories for the original parameters and the trials parameters. This depends on the number of patterns K. Furthermore, the parameters can be presented by SA algorithm with high precision since we do not need to quantize the parameter space as in the traditional HT.

Preprocessing. In seismic application, we have no constraint on the center. However, for ideal case, the hyperbola has the center on x-axis, i.e. $t = 0$. In simulated seismic data, we can find that the center does not lie on the x-axis, since convolution produces a shift. So preprocessing is quite critical. Wavelet and deconvolution processing may be needed in the preprocessing to improve the detection result.

References

[1] P. V. C. Hough, "Method and means for recognizing complex patterns," U.S. Patent 3069654, 1962.

[2] R. O. Duda and P. E. Hart, "Use of Hough transform to detect lines and curves in pictures," *Communication ACM*, vol. 15, 1972, pp. 11-15.

[3] M. M. Slotnick, *Lseeons in Seismic Computing*. The Society of Exploration Geophysicists, 1959.

[4] M. B. Dobrin and C. H. Savit, *Introduction to Geophysical Prospecting*. McGraw-Hill Book Co., New York, 1988.

[5] O. Yilmaz, *Seismic data processing*. The Society of Exploration Geophysicists, 1987.

[6] P. Kearey and M. Brooks, *An Introduction to Geophysical Exploration*. Blackwall Science Publications, 1991.

[7] K. Y. Huang, K. S. Fu, T. H. Sheen, and S. W. Cheng, "Image processing of seismograms: (A) Hough transformation for the detection of seismic patterns. (B) Thinning processing in the seismogram," *Pattern Recognition*, vol. 18, no.6, pp. 429-440, 1985.

[8] J. Basak and A. Das, "Hough transform networks: learning conoidal structures in a connectionist framework," *IEEE transaction on Neural Networks*, vol. 13, 2002, pp. 381-392.

[9] K. Y. Huang, J. D. You, K. J. Chen, H. L. Lai, and A. J. Don, "Hough Transform neural network for seismic pattern detection," *International Joint Conference on Neural Networks*, July 16-21, 2006, pp. 4670-4675.

[10] S. Kirkpatrick, C. D. Gelatt, and M. P. Vecchi, "Optimization by simulated annealing," *Science*, vol. 220, 1983, pp. 671-680.

[11] N. Metropolis, A. Rosenbluth, M. Rosenbluth, A. Teller, and E. Teller, "Equation of state calculations by fast computing machines," *J Chem Phys.*, 1953, pp.1087-1092.

[12] R. W. Klein and R. C. Dubes, "Experiments in projection and clustering by simulated annealing," *Pattern Recognition*, vol. 22, 1989, pp. 213-220.

[13] D. E. Brown and C. L. Huntley, "A practical application of simulated annealing to clustering," *Pattern Recognition*, vol. 25, 1992, pp. 401-412.

[14] K. S. Al-Sultan, S. Z. Selim, "A global algorithm for the fuzzy clustering problem," *Pattern Recognition*, vol. 26, 1993, pp. 1357-1361.

[15] S. Geman and D. Geman, "Stochastic relaxation, Gibbs distribution and Bayesian restoration of images," *IEEE Trans. Pattern Analysis and Machine Intelligence*,

vol. 6, 1984, pp. 721-741.

[16] H. Szu, R. Hartley “Fast simulated annealing,” *Physics Letters A*, vol. 122, 1987, pp. 157-162.

[17] A. Corana, M. Marchesi, C. Martini, and S. Ridella, “Minimizing multimodal functions of continuous variables with the simulated annealing algorithm,” *Mathematical Software*, *ACM Transactions on*, vol. 13, 1987, pp. 262-280.

[18] G. P. Barabino, G. S. Barabino, B. Bianco, and M. Marchesi, “A study on the performance of simplex methods for function minimization,” *Circuits and Computers IEEE International Conference on*, ICCC 80, 1980, pp. 1150-1153.

[19] S. F. Masri, G. A. Bekey, F. B. Safford, “Global Optimization Algorithm Using Adaptive Random Search,” *appl. Math*. *and Comput.* vol. 7, 1980, pp. 353-376.